LETTER

doi:10.1038/nature24660

Orthogonal muscle fibres have different instructive roles in planarian regeneration

M. Lucila Scimone[1,2,3], Lauren E. Cote[1,2,3] & Peter W. Reddien[1,2,3]

The ability to regenerate missing body parts exists throughout the animal kingdom. Positional information is crucial for regeneration, but how it is harboured and used by differentiated tissues is poorly understood. In planarians, positional information has been identified from study of phenotypes caused by RNA interference in which the wrong tissues are regenerated. For example, inhibition of the Wnt signalling pathway leads to regeneration of heads in place of tails[1–3]. Characterization of these phenotypes has led to the identification of position control genes (PCGs)—genes that are expressed in a constitutive and regional manner and are associated with patterning. Most PCGs are expressed within planarian muscle[4]; however, how muscle is specified and how different muscle subsets affect regeneration is unknown. Here we show that different muscle fibres have distinct regulatory roles during regeneration in the planarian *Schmidtea mediterranea*. *myoD* is required for formation of a specific muscle cell subset: the longitudinal fibres, oriented along the anterior–posterior axis. Loss of longitudinal fibres led to complete regeneration failure because of defects in regeneration initiation. A different transcription factor-encoding gene, *nkx1-1*, is required for the formation of circular fibres, oriented along the medial–lateral axis. Loss of circular fibres led to a bifurcated anterior–posterior axis with fused heads forming in single anterior blastemas. Whereas muscle is often viewed as a strictly contractile tissue, these findings reveal that different muscle types have distinct and specific regulatory roles in wound signalling and patterning to enable regeneration.

Body wall muscle (BWM) in *S. mediterranea* consists of multiple fibres with different orientations (Fig. 1a; Supplementary Video 1). The outermost circular BWM layer runs along the medial–lateral axis, underneath the subepidermal membrane. Below, there is a diagonal and thin longitudinal muscle fibre network, and an innermost layer comprised of thick longitudinal fibres running along the anterior–posterior axis[5,6] (Supplementary Video 1).

MyoD, a basic helix–loop–helix transcription factor, has conserved roles in myogenesis[7], acting in vertebrates with Myf5 and Mrf4 to generate skeletal muscle[8]. In *Caenorhabditis elegans*, the *myoD* homologue *hlh-1* synergizes with *unc-120* and *hnd-1* to orchestrate body wall myogenesis[9]. In *Drosophila*, by contrast, the *myoD* homologue *nau* is required for differentiation of a limited number of muscles[10]. Using fluorescent *in situ* hybridization (FISH), we found that planarian *myoD* was primarily expressed in *collagen*$^+$ BWM cells (Fig. 1b); a minor *myoD*$^+$ cell fraction co-expressed the neoblast (proliferating cell) marker *smedwi-1* (Extended Data Fig. 1a). Notably, only 46% of BWM cells expressed *myoD*, raising the possibility that *myoD* expression is specific to a muscle cell subset or to a transient differentiation stage.

RNA interference (RNAi) of *myoD* caused animals to become longer and thinner (Fig. 1c; Extended Data Fig. 1b). BWM cells (*collagen*$^+$) were substantially decreased in uninjured *myoD*(*RNAi*) animals, whereas intestinal muscle was unperturbed (Extended Data Fig. 1c). Immunostainings showed that *myoD*(*RNAi*) animals had a marked loss of only a subset of BWM: longitudinal fibres were lost whereas circular and diagonal fibres remained normal (Fig. 1d; Extended Data Fig. 1d; Supplementary Video 2). Electron microscopy confirmed this longitudinal fibre-specific phenotype (Fig. 1e).

RNA sequencing (RNA-seq) in uninjured *myoD*(*RNAi*) animals showed a muscle-specific gene expression reduction (Extended Data Fig. 1e, f; Supplementary Table 1). Other genes encoding conserved transcription factors (*snail*, *lbx*, *nkx6-2* and *lhx2/9*) also displayed decreased expression (Fig. 1f; Extended Data Fig. 1g; Supplementary Table 1). These genes were expressed in BWM and, at least partially, with *myoD* (Extended Data Fig. 2a–e). RNAi of *snail*, *lbx* or *nkx6-2* did not cause major muscle phenotypes (Extended Data Fig. 2f), but these transcription factors might regulate longitudinal fibre biology. A subset of PCGs were co-expressed with *myoD* and were significantly (adjusted P value < 0.01) reduced in *myoD*(*RNAi*) animals (Fig. 1f, g; Extended Data Fig. 3; Extended Data Table 1; Supplementary Table 1), indicating that some patterning genes are predominantly expressed in longitudinal muscle fibres.

We used *myoD* RNAi to examine the role of longitudinal fibres in regeneration. Previous studies showed a range of regeneration defects in *myoD*(*RNAi*) animals, such as pointed blastemas (regenerative outgrowths), for unknown reasons[11,12]. We optimized a *myoD* RNAi protocol that resulted in an essentially complete block of regeneration following amputation (Fig. 2a). These animals contracted wounds (Extended Data Fig. 4a), but failed to regenerate the anterior (*notum*$^+$) or posterior (*wnt1*$^+$) poles (Extended Data Fig. 4b, c), which are essential for blastema patterning[13–15].

Planarian regeneration and tissue turnover require neoblasts—proliferating cells that include pluripotent stem cells. Accordingly, numerous abnormalities in regeneration can be explained by neoblast defects. Regeneration failure in *myoD*(*RNAi*) animals, however, was not caused by a general neoblast dysfunction. Neoblasts differentiated into neurons (*chat*$^+$) and muscle (*collagen*$^+$) in fragments of *myoD*(*RNAi*) animals that failed to regenerate 30 days after head and tail amputation (Fig. 2b); however, neoblasts in these headless fragments did not generate eye progenitors (Extended Data Fig. 4d). Moreover, *myoD*(*RNAi*) animals regenerated eyes following eye resection (Extended Data Fig. 4e), a small injury that does not elicit sustained neoblast proliferation or require restoration of missing positional information for repair, but still requires neoblast differentiation[16]. In conclusion, *myoD*(*RNAi*) animals were fully capable of generating new tissues during tissue turnover and small injury repair, but failed to regenerate missing tissues following amputation.

Regeneration in planarians involves several phases. There is an initial wound response, occurring at essentially all injuries, that is associated with rapid wound-induced gene expression (3–12 h post-wounding)[17,18]. Subsequently, and only with injuries where substantial tissue has been removed, additional events occur that collectively comprise the regenerative response (approximately 24–48 h

[1]Howard Hughes Medical Institute, Massachusetts Institute of Technology, Cambridge, Massachusetts 02139, USA. [2]Whitehead Institute for Biomedical Research, 9 Cambridge Center, Cambridge, Massachusetts 02142, USA. [3]Department of Biology, Massachusetts Institute of Technology, Cambridge, Massachusetts 02139, USA.

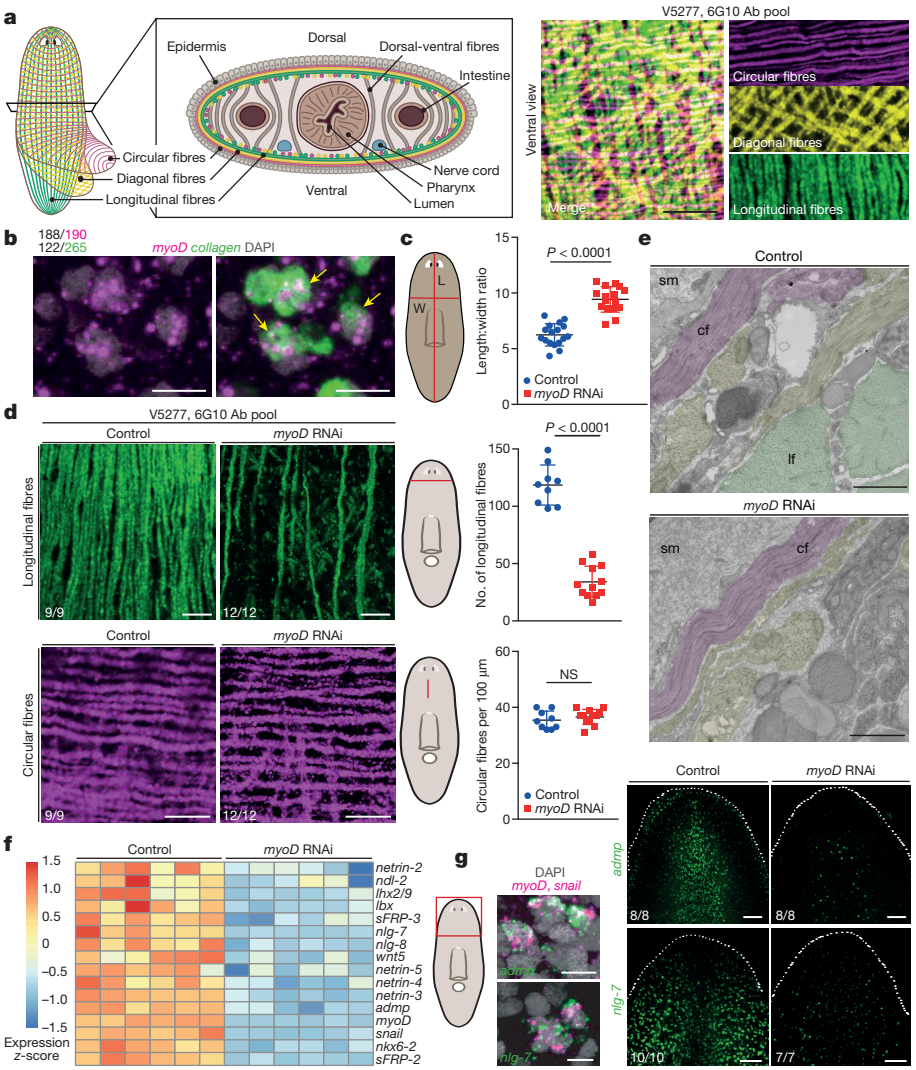

Figure 1 | *myoD* specifies longitudinal muscle fibres. a, Diagram and immunofluorescence showing BWM layers (five animals, two experiments). **b**, *myoD* and BWM *collagen*$^{+}$ cells (five animals, two experiments). White, double-positive cells from one animal. Ab, antibody. **c**, Length (L)-to-width (W) ratio (17 control and 16 *myoD* RNAi animals, three experiments). **d**, Immunofluorescence showing longitudinal fibre loss in *myoD*(*RNAi*) animals (three experiments). **e**, Transmission electron microscopy (TEM) showing longitudinal fibre reduction in *myoD*(*RNAi*) animals (two animals). Pseudocoloured circular (cf), longitudinal (lf), and other fibres (yellow); sm, subepidermal membrane. **f**, Heat map of transcription factor and PCG expression downregulation after *myoD* RNAi (adjusted *P* value < 0.01; six replicates, one animal per replicate). **g**, Co-expression of *myoD* and *snail* with PCGs, and loss of PCG expression after *myoD* RNAi (two experiments). Cartoon line shows measurement site. Animals uninjured, 10 double-stranded RNA (dsRNA) feedings. *P* values determined by two-tailed Student's *t*-test. Data are mean ± s.d. NS, not significant. Bottom left numbers in images show animals with phenotype out of total tested. Scale bars, 10 µm (**a**, **b**, **d**, **g**, left); 1 µm (**e**); 100 µm (**g**, right).

post-amputation (hpa)). These events include persistent wound-induced gene expression, patterning gene expression domain regeneration in muscle, sustained neoblast proliferation and accumulation at wounds, and body-wide elevated apoptosis[17–20]. Soon after these changes, new differentiated cell types emerge (about 72 hpa) and blastema growth and patterning ensue. Because of the striking regeneration failure in *myoD*(*RNAi*) animals, we reasoned that some aspect of these early regeneration steps is likely to require *myoD* and/or longitudinal muscle fibres.

Many planarian wound-induced genes are expressed in the epidermis, neoblasts, or muscle[17,18]. *myoD* was not required for epidermis, neoblast, or most muscle wound-induced (6 hpa) gene expression (*wntless*, *inhibin-1*, *wnt1* and *nlg-1*) (Extended Data Fig. 4f). However, a marked reduction in muscle wound-induced expression of *notum* and *fst* (which encodes Follistatin) was observed in *myoD*(*RNAi*) animals at multiple time points post-amputation and concomitantly with loss of longitudinal fibres (Fig. 2c; Extended Data Fig. 4g). Furthermore, wound-induced expression of *fst* and *notum* was greatly enriched in *myoD*$^{+}$ cells (Fig. 2d), compared to other muscle wound-induced genes (Extended Data Fig. 5a). These data indicate that *notum* and *fst* are unique among wound-induced genes in that their expression is restricted to longitudinal fibres.

The effect of *myoD* RNAi on *fst* and *notum* was particularly revealing, because these genes have critical roles in regeneration. *notum* encodes a Wnt-inhibitory deacylase[21,22] and controls the planarian head-versus-tail decision following amputation[23]. *notum* is preferentially expressed at anterior rather than posterior-facing wounds[17,23]. *fst* encodes a TGFβ inhibitor that is required for sustained wound-induced gene expression and elevated neoblast proliferation during the regenerative response[24]. *fst* RNAi[24,25], like *myoD* RNAi, resulted in failure of regeneration but allowed tissue turnover.

To further assess similarities between the *myoD* and *fst* RNAi phenotypes, we performed RNA-seq on anterior-facing wounds during the wound and regenerative responses (Supplementary Table 1). Most wound-induced genes were expressed normally following *myoD* and *fst* RNAi at 6 hpa. However, at later time points

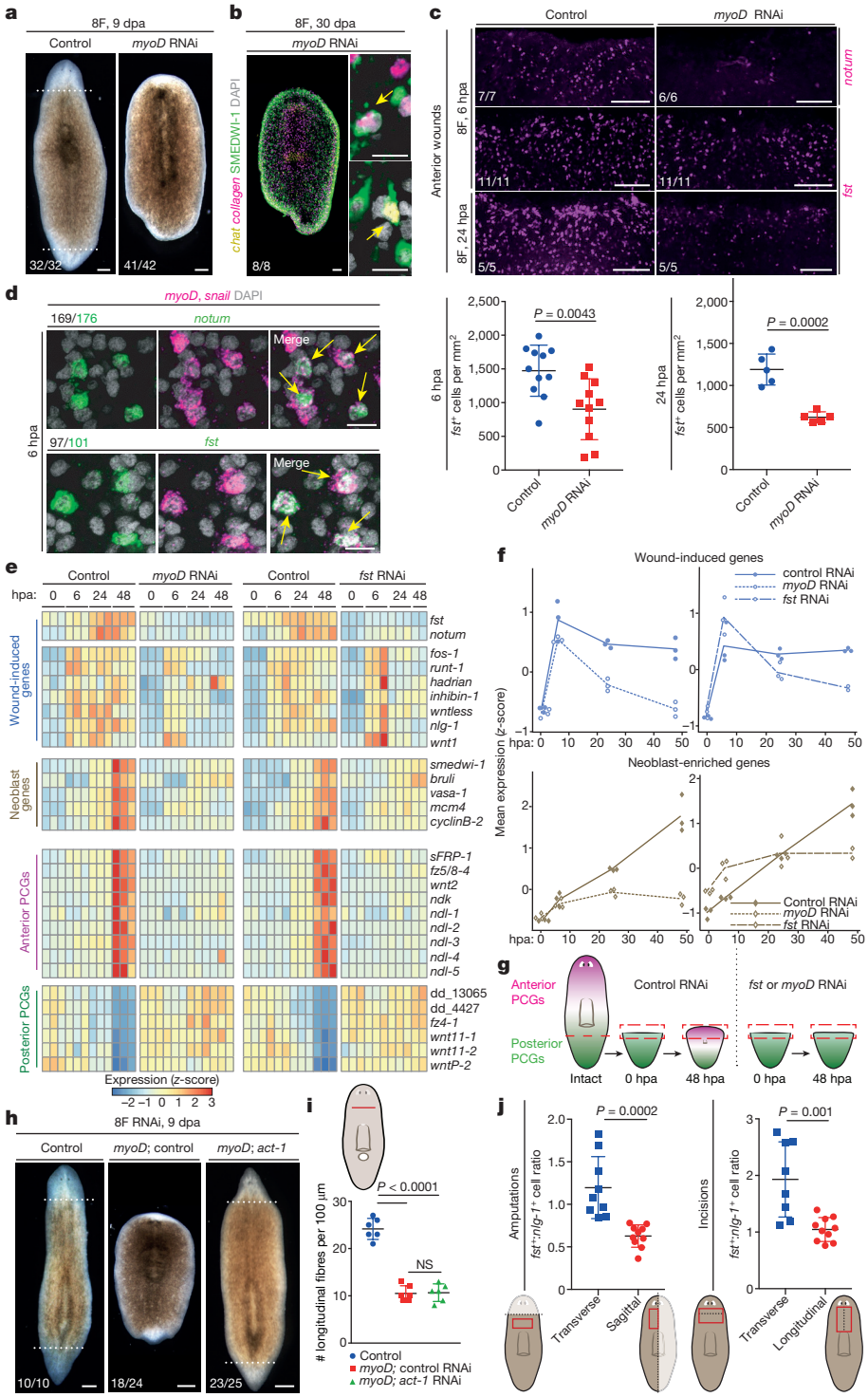

Figure 2 | *myoD* is required for regeneration initiation. a, Lack of regeneration after eight *myoD* dsRNA feedings (8F, four experiments). **b**, New neurons (*chat*$^+$) and muscle (*collagen*$^+$) in non-regenerative *myoD* RNAi fragments (two experiments). **c**, Reduced *notum* and *fst* expression in *myoD* RNAi animals (two experiments). **d**, Cells expressing *myoD*, *snail* and *notum* or *fst* at anterior-facing wounds (five animals per FISH, two experiments, white: double-positive cells from one animal). **e**, RNA-seq data heat map (three replicates per time point, five animal wounds per replicate). **f**, Mean expression *z*-score from **e** of all wound-induced and neoblast genes[17]. **g**, Cartoon showing positional information in regeneration. **h**, *act-1* inhibition suppressed regeneration failure in *myoD* RNAi animals (three experiments). **i**, Quantification of longitudinal fibres (six animals per group, two experiments). One-way ANOVA, post Dunnett's test. **j**, Higher *fst*$^+$ to *nlg-1*$^+$ cell ratio in transverse ($n = 9$ and 8) versus sagittal ($n = 10$ and 10) amputations and incisions, respectively, at 6 hpa. Dotted line, injury or amputation site; red outline, measurement site. Two-tailed Student's *t*-test (**c**, **j**), all mean ± s.d. Bottom left number, animals with phenotype of total tested. Scale bars, 100 µm (**a**, **b**, left, **c**, **h**); 10 µm (**b**, right, **d**).

(24–48 hpa, regenerative response) expression of 75 out of 128 wound-induced genes was significantly lower (adjusted $P < 0.01$) after *myoD* RNAi than in controls and 24 out of 128 were lower in both *myoD* and *fst* RNAi conditions (Fig. 2e, f; Extended Data Fig. 5b).

Sustained neoblast proliferation and accumulation at wounds (at around 48 hpa), detected as increased neoblast signature transcripts at wounds, was lacking in *myoD* and *fst* RNAi animals (Fig. 2e, f; Extended Data Fig. 5c).

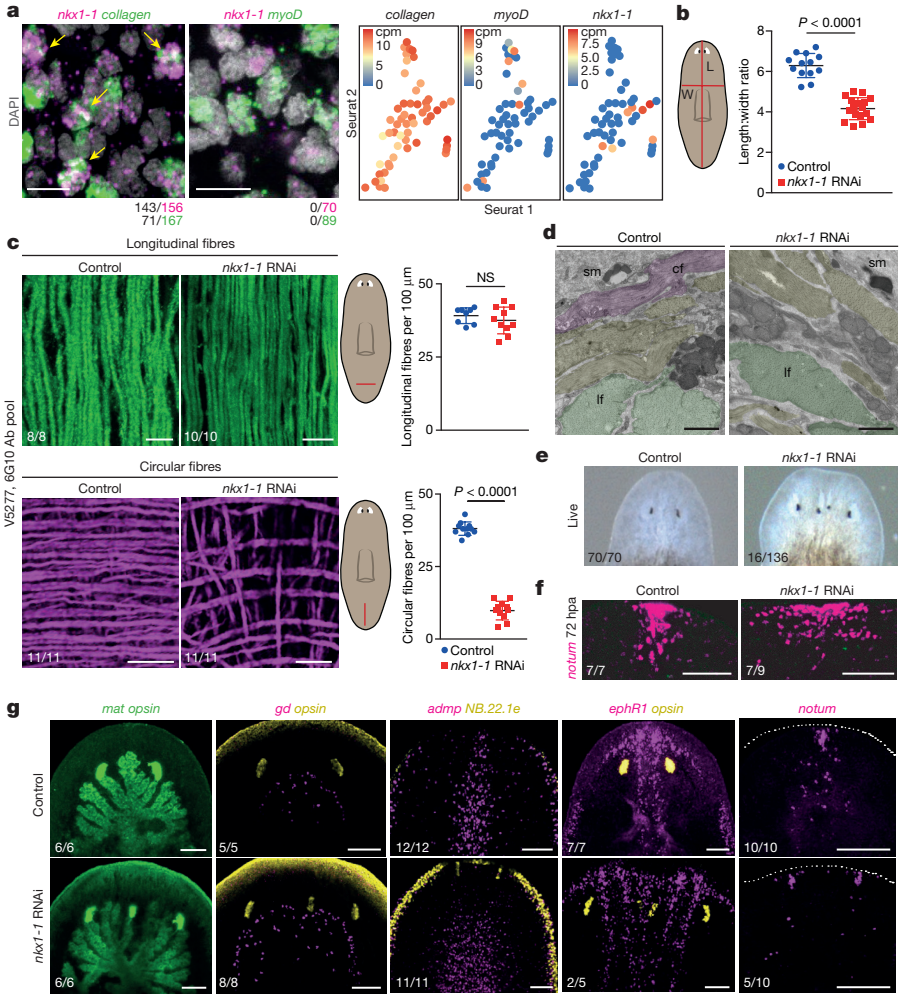

Figure 3 | *nkx1-1* specifies circular muscle fibres and is required for medial–lateral patterning. a, *nkx1-1*$^+$ and BWM *collagen*$^+$ cells (white, double-positive cells from one animal) and mutually exclusive expression of *nkx1-1* and *myoD* shown by FISH (four animals, two experiments) and single-cell (each dot) RNA-seq[17]. **b**, Length-to-width ratio (13 control and 17 *nkx1-1* RNAi animals, three experiments). **c**, **d**, Circular fibre loss after *nkx1-1* RNAi shown by immunofluorescence (**c**, three experiments) and pseudocoloured TEM (**d**, two animals). **e**, Medial–lateral patterning defects after *nkx1-1* RNAi (four experiments). **f**, Increase in width of anterior poles (two experiments). **g**, Ectopic eyes (*opsin*$^+$), supernumerary gut branches (*mat*$^+$), wider cephalic-ganglia arc (*gd*$^+$, *glutamate decarboxylase*$^+$), wider midline (*admp*$^+$), duplicated midline (*ephR1*$^+$), and anterior poles (*notum*$^+$) in 9 dpa *nkx1-1*(*RNAi*) animals (three experiments). Cartoon line, measurement site. Animals had 12 dsRNA feedings. Two-tailed Student's *t*-test, mean ± s.d.; NS, not significant (**b**, **c**). Bottom left number: animals with phenotype of total tested. Scale bars, 10 µm (**a**, **c**); 1 µm (**d**); 100 µm (**f**, **g**).

We next assessed positional information regeneration in *myoD*(*RNAi*) animals. Immediately after amputation, tail fragments express only posterior PCGs. By 48 hpa, posterior PCG expression becomes restricted posteriorly and anterior PCG expression is initiated to reconstitute normal PCG expression domains. PCG expression domain regeneration in muscle did not occur in either *myoD* or *fst* RNAi animals[26] (Fig. 2e, g; Extended Data Fig. 6a). We conclude that *myoD* and longitudinal muscle fibres are required for the regenerative response.

Follistatin negatively regulates activins (TGFβ signalling ligands), and inhibition of *activin* genes suppresses the regeneration defect in *fst*(*RNAi*) animals[24,25]. To test whether failed *fst* expression contributes to the regeneration failure in *myoD*(*RNAi*) animals, we inhibited both *myoD* and *act-1* (which encodes Activin-1). After short-term RNAi of both *myoD* and *act-1*, 23 of 25 trunk fragments regenerated (with 9 of those 23 being cyclopic) versus 6 of 24 trunk fragments after RNAi of *myoD* and control (Fig. 2h). Regeneration included re-scaling of PCG expression and anterior pole generation (Extended Data Fig. 6b). Reduced longitudinal fibre numbers and expression of *snail* (a *myoD* target) were comparable in *myoD* and *act-1* double RNAi animals and in *myoD* and control double RNAi animals (Fig. 2i; Extended Data Fig. 6c). Following long-term *myoD* RNAi, *act-1* inhibition did not rescue regeneration (Extended Data Fig. 6d), suggesting that some longitudinal muscle fibres are required for blastema formation. RNAi targeting of *β-cat-1* (which encodes β-catenin-1) causes ectopic head regeneration at wounds[1–3], but did not restore head regeneration following *myoD* RNAi (Extended Data Fig. 6e). The *act-1* suppression data demonstrate that failed regeneration in *myoD*(*RNAi*) animals is not explained simply by a dysfunction in muscle contractility, but instead by a regulatory role of longitudinal muscle fibres at wounds.

Because wound-induced *fst* expression was specific to longitudinal fibres, transverse wounds might elicit more *fst* expression than sagittal wounds. This was true for *fst*, but not for wound-induced genes that were not specific to longitudinal fibres (Fig. 2j; Extended Data Fig. 7a, b). Moreover, sagittally amputated *myoD*(*RNAi*) animals showed variable regeneration defects (Extended Data Fig. 7c).

Our results demonstrate an essential and specific role for a particular muscle fibre class in regeneration. This raises the question of how other muscle fibres are specified, and whether they have other regeneration roles. We mined previously reported single-muscle-cell RNA-seq data[27] and identified a muscle-expressed gene (*nkx1-1*) encoding an NK1 homeodomain transcription factor homologous to *Drosophila*

slouch (encoded by *slou*) (Extended Data Fig. 1g). Like *nau, slou* is required for the formation of a subset of *Drosophila* muscles[28]. Like *myoD*, *nkx1-1* was predominantly expressed in *collagen*$^+$ BWM cells, with a minor fraction expressed in neoblasts (Fig. 3a; Extended Data Fig. 8a, b). *nkx1-1* was expressed in a subset of BWM cells (43%) distinct from *myoD*$^+$ cells (Fig. 3a; Extended Data Fig. 2e), suggesting that these genes have roles in different muscle cell subsets.

Whereas *myoD* inhibition resulted in thinner animals, *nkx1-1* RNAi resulted in wider animals (Fig. 3b; Extended Data Fig. 8c). *nkx1-1*(*RNAi*) animals displayed a marked reduction in circular fibres, whereas longitudinal and diagonal fibres remained essentially unaffected (Fig. 3c; Extended Data Fig. 8d, e; Supplementary Video 3). Electron microscopy confirmed this circular fibre-specific phenotype (Fig. 3d). RNA-seq analysis of *nkx1-1*(*RNAi*) animals detected a general reduction in muscle-specific gene expression similar to that seen in *myoD*(*RNAi*) animals (Extended Data Fig. 8f). Most PCGs were unaffected (Supplementary Table 1) and single-muscle-cell RNA-seq showed that they were not exclusively expressed in *nkx1-1*$^+$ muscle cells (Extended Data Fig. 2e). Extensive FISH analysis (Extended Data Table 1), however, revealed that *wnt11-1* was predominantly expressed in *nkx1-1*$^+$ cells and that expression of *wnt11-1* and *act-2* (which encodes Activin-2), was reduced in *nkx1-1*(*RNAi*) animals (Extended Data Fig. 8g).

To identify the role of *nkx1-1* and circular muscle fibres in regeneration, RNAi animals were subjected to head and tail amputation. *nkx1-1*(*RNAi*) trunk fragments contracted wounds normally and regenerated heads with widely spaced eyes and indented tails (Extended Data Fig. 9a, b). Some *nkx1-1*(*RNAi*) animals regenerated a bifurcated anterior–posterior axis with two merged heads within a single blastema (Fig. 3e). Head blastemas had numerous abnormalities (Fig. 3f, g), including ectopic eyes, supernumerary ectopic gut branches, and wider cephalic ganglia than normal (Fig. 3g; Extended Data Fig. 9c). An ectopic brain lobe occasionally formed (Supplementary Videos 4, 5). In addition, animals displayed broader midline gene expression domains and, in extreme cases, midline duplication with duplicated anterior poles (Fig. 3g).

At 72 hpa, all *nkx1-1*(*RNAi*) animals had markedly wider regenerating anterior poles (Fig. 3f), suggesting that wider regenerating poles coalesced into two independent anterior poles. These 72-h blastemas showed aberrant muscle fibre organization, with reduced circular fibres and a lack of constricted muscle fibres towards the pole (Extended Data Fig. 9d). Because the pole acts as an organizer to promote midline regeneration, a plane around which bilateral symmetry is established[13], we suggest that split anterior poles organize the formation of two midlines, explaining the duplication of heads in *nkx1-1*(*RNAi*) animals. These animals regenerated after sagittal amputations with a similar abnormal phenotype (Extended Data Fig. 9e).

Because planarian muscle provides positional information that is required for patterning, muscle fibre loss might result in aberrant patterning during tissue turnover. Inhibition of both *myoD* and *nkx1-1* with RNAi resulted in a marked reduction in BWM fibres but not other muscle types (Fig. 4a; Extended Data Fig. 10a–d; Supplementary Video 6). These animals had ectopic posterior eyes (Fig. 4a), indicating that exclusive BWM disruption is sufficient to affect normal patterning. Expression of several PCGs was defective in animals in which both *myoD* and *nkx1-1* were inhibited (Fig. 4b; Extended Data Fig. 10e), including *ndk*, *ndl*, and *fz5/8-4* genes (encoding Nou darake, Nou darake-like proteins, and Frizzled5/8-4, respectively), which are required for eye patterning[27]. Animals in which both *myoD* and *nkx1-1* were inhibited eventually lysed by 12–20 weeks of RNAi (Extended Data Fig. 10f, g), indicating that BWM loss led to disruption of body integrity.

In conclusion, we have demonstrated that different planarian muscle fibres have distinct regulatory roles in regeneration. *myoD*, which encodes a homologue of a well-characterized vertebrate myogenic factor, does not have a general role in planarian myogenesis.

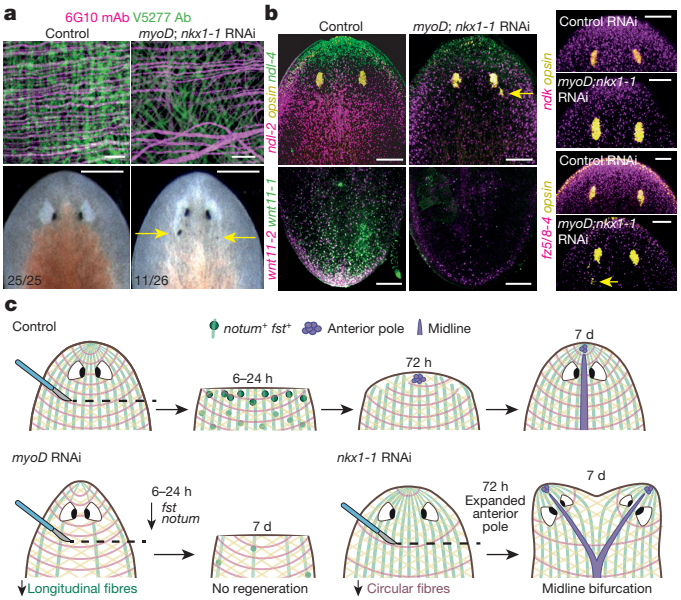

Figure 4 | Double *myoD* and *nkx1-1* RNAi animals have patterning defects. a, BWM loss (ten animals per group) and patterning defects (arrows, ectopic eyes) in double *myoD* and *nkx1-1* RNAi animals (three experiments). **b**, Reduced PCG expression in double *myoD* and *nkx1-1* RNAi animals (four animals per FISH, two experiments). Bottom left number, animals with phenotype of total tested. **c**, Model showing how different muscle fibre subsets have distinct roles during regeneration. Longitudinal fibres are required to initiate the regenerative response and circular fibres are essential for normal medial–lateral patterning. Scale bars, 10 μm (**a**, top); 500 μm (**a**, bottom); 100 μm (**b**).

Instead, *myoD* specifies a subset of BWM cells: the longitudinal fibres (Fig. 4c). A second transcription factor-encoding gene, *nkx1-1*, specified another subset of planarian BWM cells: the circular fibres. Our results suggest that in planarians, as in *Drosophila*, different transcription factors specify distinct muscle subsets. These genes provided tools to reveal distinct roles for longitudinal and circular muscle fibres. Circular fibres were required for proper medial–lateral regeneration, with two heads emerging instead of one after a reduction in circular fibres. Longitudinal fibres were required to initiate the regeneration program. Animals lacking longitudinal fibres could not reestablish positional information in muscle and lacked stem cell responses to injury, despite being fully capable of tissue turnover. Simultaneous loss of both fibre classes led to homeostatic patterning defects. We conclude that, in addition to contraction, different muscle fibres have specific regulatory roles in orchestrating regeneration in planarians.

Online Content Methods, along with any additional Extended Data display items and Source Data, are available in the online version of the paper; references unique to these sections appear only in the online paper.

Received 2 May; accepted 20 October 2017.
Published online 22 November 2017.

1. Petersen, C. P. & Reddien, P. W. *Smed-βcatenin-1* is required for anteroposterior blastema polarity in planarian regeneration. *Science* **319,** 327–330 (2008).
2. Gurley, K. A., Rink, J. C. & Sánchez Alvarado, A. β-catenin defines head versus tail identity during planarian regeneration and homeostasis. *Science* **319,** 323–327 (2008).
3. Iglesias, M., Gomez-Skarmeta, J. L., Saló, E. & Adell, T. Silencing of *Smed-βcatenin-1* generates radial-like hypercephalized planarians. *Development* **135,** 1215–1221 (2008).
4. Witchley, J. N., Mayer, M., Wagner, D. E., Owen, J. H. & Reddien, P. W. Muscle cells provide instructions for planarian regeneration. *Cell Reports* **4,** 633–641 (2013).
5. Cebrià, F., Vispo, M., Newmark, P., Bueno, D. & Romero, R. Myocyte differentiation and body wall muscle regeneration in the planarian *Girardia tigrina*. *Dev. Genes Evol.* **207,** 306–316 (1997).

6. Cebrià, F. Planarian body-wall muscle: Regeneration and function beyond a simple skeletal support. *Front. Cell Dev. Biol.* **4,** 8 (2016).
7. Buckingham, M. & Rigby, P. W. Gene regulatory networks and transcriptional mechanisms that control myogenesis. *Dev. Cell* **28,** 225–238 (2014).
8. Kassar-Duchossoy, L. *et al.* Mrf4 determines skeletal muscle identity in *Myf5:Myod* double-mutant mice. *Nature* **431,** 466–471 (2004).
9. Baugh, L. R. & Hunter, C. P. MyoD, modularity, and myogenesis: conservation of regulators and redundancy in *C. elegans*. *Genes Dev.* **20,** 3342–3346 (2006).
10. Balagopalan, L., Keller, C. A. & Abmayr, S. M. Loss-of-function mutations reveal that the *Drosophila nautilus* gene is not essential for embryonic myogenesis or viability. *Dev. Biol.* **231,** 374–382 (2001).
11. Reddien, P. W., Bermange, A. L., Murfitt, K. J., Jennings, J. R. & Sánchez Alvarado, A. Identification of genes needed for regeneration, stem cell function, and tissue homeostasis by systematic gene perturbation in planaria. *Dev. Cell* **8,** 635–649 (2005).
12. Cowles, M. W. *et al.* Genome-wide analysis of the bHLH gene family in planarians identifies factors required for adult neurogenesis and neuronal regeneration. *Development* **140,** 4691–4702 (2013).
13. Scimone, M. L., Lapan, S. W. & Reddien, P. W. A forkhead transcription factor is wound-induced at the planarian midline and required for anterior pole regeneration. *PLoS Genet.* **10,** e1003999 (2014).
14. Vogg, M. C. *et al.* Stem cell-dependent formation of a functional anterior regeneration pole in planarians requires Zic and Forkhead transcription factors. *Dev. Biol.* **390,** 136–148 (2014).
15. Vásquez-Doorman, C. & Petersen, C. P. *zic-1* expression in planarian neoblasts after injury controls anterior pole regeneration. *PLoS Genet.* **10,** e1004452 (2014).
16. LoCascio, S. A., Lapan, S. W. & Reddien, P. W. Eye absence does not regulate planarian stem cells during eye regeneration. *Dev. Cell* **40,** 381–391.e3 (2017).
17. Wurtzel, O. *et al.* A generic and cell-type-specific wound response precedes regeneration in planarians. *Dev. Cell* **35,** 632–645 (2015).
18. Wenemoser, D., Lapan, S. W., Wilkinson, A. W., Bell, G. W. & Reddien, P. W. A molecular wound response program associated with regeneration initiation in planarians. *Genes Dev.* **26,** 988–1002 (2012).
19. Wenemoser, D. & Reddien, P. W. Planarian regeneration involves distinct stem cell responses to wounds and tissue absence. *Dev. Biol.* **344,** 979–991 (2010).
20. Pellettieri, J. *et al.* Cell death and tissue remodeling in planarian regeneration. *Dev. Biol.* **338,** 76–85 (2010).
21. Kakugawa, S. *et al.* Notum deacylates Wnt proteins to suppress signalling activity. *Nature* **519,** 187–192 (2015).
22. Zhang, X. *et al.* Notum is required for neural and head induction via Wnt deacylation, oxidation, and inactivation. *Dev. Cell* **32,** 719–730 (2015).
23. Petersen, C. P. & Reddien, P. W. Polarized *notum* activation at wounds inhibits Wnt function to promote planarian head regeneration. *Science* **332,** 852–855 (2011).
24. Gaviño, M. A., Wenemoser, D., Wang, I. E. & Reddien, P. W. Tissue absence initiates regeneration through Follistatin-mediated inhibition of Activin signaling. *eLife* **2,** e00247 (2013).
25. Roberts-Galbraith, R. H. & Newmark, P. A. Follistatin antagonizes Activin signaling and acts with Notum to direct planarian head regeneration. *Proc. Natl Acad. Sci. USA* **110,** 1363–1368 (2013).
26. Adler, C. E. & Sánchez Alvarado, A. PHRED-1 is a divergent neurexin-1 homolog that organizes muscle fibers and patterns organs during regeneration. *Dev. Biol.* **427,** 165–175 (2017).
27. Scimone, M. L., Cote, L. E., Rogers, T. & Reddien, P. W. Two FGFRL-Wnt circuits organize the planarian anteroposterior axis. *eLife* **5,** e12845 (2016).
28. Knirr, S., Azpiazu, N. & Frasch, M. The role of the NK-homeobox gene *slouch* (S59) in somatic muscle patterning. *Development* **126,** 4525–4535 (1999).

Supplementary Information is available in the online version of the paper.

Acknowledgements We thank N. Watson and A. Mahowald for transmission electron microscopy; S. LoCascio for eye resections; C.-C. Chen for V5277; and M. Fedorovsky for illustrations. We acknowledge support from NIH R01GM080639 and the Eleanor Schwartz Charitable Foundation. P.W.R. is an Investigator of the HHMI and an associate member of the Broad Institute of Harvard and MIT.

Author Contributions M.L.S. and L.E.C. carried out RNAi characterization, RNA-seq and TEM; L.E.C. carried out phylogenetic analysis; M.L.S., L.E.C. and P.W.R. discussed the data and wrote the paper.

Author Information Reprints and permissions information is available at www.nature.com/reprints. The authors declare no competing financial interests. Readers are welcome to comment on the online version of the paper. Publisher's note: Springer Nature remains neutral with regard to jurisdictional claims in published maps and institutional affiliations. Correspondence and requests for materials should be addressed to P.W.R. (reddien@wi.mit.edu).

Reviewer Information *Nature* thanks C. Petersen and A. Sánchez Alvarado for their contribution to the peer review of this work.

METHODS

Animals. Asexual *Schmidtea mediterranea* (strain CIW4) animals were used and starved for 7–14 days before experiments. Animals for all experiments were randomly selected from a large collection of clonal animals. Investigators were not blinded during data collection and analysis.

RNA-seq experiments. Total RNA was isolated using Trizol (Life Technologies) from single animals (uninjured *myoD* and *nkx1-1* RNAi animals) or five pooled anterior wound sites from tail fragments (*myoD* and *fst* timecourse). Biological triplicates of pooled wound sites were used as described previously[17] and for whole animal RNA-seq, six animals were used instead to increase statistical power. Libraries were prepared using the Kapa Stranded mRNA-Seq Kit Illumina Platform (KapaBiosystems). Libraries were sequenced on an Illumina Hi-Seq. The fst_00_48_wiF_1 library was removed from further analysis because of high human sequence contamination. Libraries were mapped to the dd_Smed_v4 transcriptome[29] (http://planmine.mpi-cbg.de) using bowtie 1[30] with -best alignment parameter. Reads from the same isotig were summed to generate raw read counts for each transcript. Pairwise differential expression analysis was performed using DESeq[31]. Expression values from DESeq normalization were scaled to generate *z*-scores for heat maps and these *z*-scores were averaged for sets of genes[17] (area under the curve (AUC) >0.80) for summary figures. Pheatmap was used to generate scaled heat maps.

Gene cloning and whole-mount *in situ* hybridizations. *nkx1-1* was amplified using the following primers: forward 5′ ATTCCAAGTCAAACGATAAGCCT; reverse 5′ TTCCGTTGGTATTTCTTTAACGG and *myoD* was amplified using the following primers: forward 5′ TCAACAATACCGATCCAGCCC; reverse 5′ TCGGGCTTAGCGTCCATTG. Both constructs were cloned from cDNA into the pGEM vector (Promega). These constructs were used to synthesize RNA probes and dsRNA for RNAi experiments. RNA probes were synthesized and whole-mount FISH was performed as described[27]. Light images were taken with a Zeiss Discovery Microscope. Fluorescent images were taken with a Zeiss LSM700 Confocal Microscope using ZEN software. Co-localization analyses of FISH signals were performed using Fiji/ImageJ. For each channel, histograms of fluorescence intensity were used to determine the cut-off between signal and background. All FISH images shown are maximal intensity projections and are representative of all images taken in each condition.

RNAi. dsRNA was prepared from *in vitro* transcription reactions (Promega) using PCR-generated templates with flanking T7 promoters, followed by ethanol precipitation, and annealed after resuspension in water. The concentration of dsRNA varied in each prep between 4 and 7 μg/ml. dsRNA was then mixed with planarian food (liver)[32] and 2 μl of this mixture per animal (liver containing dsRNA) was used for feedings. For homeostasis experiments, the following feeding protocol was used: animals were fed six times in three weeks, and then fed four to ten times once a week. Animals were then fixed seven days after the last feeding. For regeneration experiments, animals were fed twice a week with the total number of RNAi feedings being variable depending on the experiment (indicated in the Figures) and were then amputated into three pieces (head, trunk and tail pieces) one week after the last RNAi feeding. Seven or nine days after amputation, trunk pieces were scored, and fixed for further analysis. For sagittal amputations, regenerating animals were scored 11 days after amputation. For all RNAi conditions tested, the total amount of dsRNA per feeding per animal was kept constant, as described[27]. For RNA-seq experiments in intact animals, control, *myoD*, and *nkx1-1* RNAi animals were fed 10 times; for wound-induced RNA-seq experiments, control and *myoD*(*RNAi*) animals were fed eight times in four weeks, and control and *fst* RNAi animals were fed six times in three weeks. For the *β-cat-1* suppression experiment, *myoD*(*RNAi*) animals were fed six times in three weeks and one extra feeding of either control or *β-cat-1* dsRNA was performed in the third week. Animals were then amputated on the day of the last feeding and scored at different time points as indicated. Visual estimation of preliminary experiments indicated large effect sizes with greater than twofold differences in number of fibres and length-to-width ratios, therefore a minimum sample size of 6 was chosen to give a 99% power with a 1% false positive error rate. This size estimation applies for measurements taken in Figs 1c, d, 2i, 3b, c and Extended Data Figs 4g, 9b, 10f.

Immunostainings. Animals were fixed as for *in situ* hybridizations and then treated as described[27]. An anti-muscle mouse monoclonal antibody 6G10[33] was used in a 1:1,000 dilution, an anti-muscle rabbit polyclonal antibody V5277 (identified from reactivity of serum to muscle from an animal injected with a peptide from an unrelated protein, Cintillo) was used in a 1:500 dilution, and an anti-mouse or anti-rabbit Alexa conjugated antibody (Life Tech) was used in a 1:500 dilution.

Phylogenetic analysis. NKX and Netrin trees show 105 homeobox and 20 Netrin family proteins, respectively, from diverse organisms. Trees were based on previous reports[34,35]. Protein sequences were aligned using MUSCLE with default settings and trimmed with Gblocks. Maximum likelihood analyses were run using PhyML with 100 or 1,000 bootstrap replicates, the WAG model of amino acid substitution, four substitution rate categories and the proportion of invariable sites estimated from the dataset. Trees were visualized in FigTree. Accession numbers of proteins used to generate the phylogenetic trees can be found in Supplementary Table 2.

Transmission electron microscopy. Animals were kept on ice for 10 min before fixation with cold 2.5% glutaraldehyde, 3% paraformaldehyde with 5% sucrose in 0.1 M sodium cacodylate buffer (pH 7.4) overnight, then post-fixed in 1% OsO_4 in veronal-acetate buffer. Animals were stained overnight with 0.5% uranyl acetate in veronal-acetate buffer (pH 6.0), dehydrated, and embedded in Spurr's resin. Transverse sections were cut on a Reichert Ultracut E microtome with a Diatome diamond knife at a thickness setting of 50 nm and then stained with 2% uranyl acetate and lead citrate. The sections were examined using a FEI Tecnai spirit at 80 kV and photographed with an AMT CCD camera. All images were taken on the ventral BWM at 6,800×. Muscle fibres were traced by hand and pseudocoloured by fibre orientation, size, and distance from the subepidermal membrane. Circular fibres were defined as the outermost layer adjacent to the subepidermal membrane with myosin fibres running sagittal to the plane of section, and pseudocoloured magenta. Longitudinal fibres on the ventral side were thick with myosin fibres transverse to the plane of section, and pseudocoloured green. All other identifiable muscle fibres were pseudocoloured yellow. For ease of visualization, smooth function (ImageJ) was applied to TEM images.

Quantifications and statistical analysis. Numbers of fibres, *fst*$^+$, and *notum*$^+$ cells were counted per animal within the regions indicated in the cartoons next to the graphs. Ratios (length to width, distance between the eyes to total length or wound-induced *fst*$^+$ to *nlg-1*$^+$ or *inhibin-1*$^+$ cells) were calculated per animal as indicated. Numbers of *fst*$^+$, *nlg-1*$^+$, or *inhibin-1*$^+$ cells at incisions were counted and normalized by wound length (in mm) using DAPI signal. Unpaired two-tailed Student's *t*-test was used to determine significant differences between two conditions, and one-way ANOVA test followed by Dunnett's multiple comparison test was used when analysing more than two conditions. Mean ± s.d. is shown in all graphs. A linear regression using all values generated from different RNAi feedings (2, 4, 8, and 11) of control and *myoD*(*RNAi*) animals was calculated in Extended Data Fig. 4g.

Data availability. RNA-seq data have been deposited in GEO with the accession number GSE99067. Gene sequences have been deposited in GenBank, accession numbers MF070478, MF070479 and MF070480. The accession numbers of reported data used in this study are PRJNA276084 (from ref. 17) and GSE74360 (from ref. 27). Accession numbers used in phylogenetic analysis are listed in Supplementary Table 2. All other data are available from the corresponding author upon reasonable request.

29. Liu, S. Y. *et al.* Reactivating head regrowth in a regeneration-deficient planarian species. *Nature* **500,** 81–84 (2013).
30. Langmead, B., Trapnell, C., Pop, M. & Salzberg, S. L. Ultrafast and memory-efficient alignment of short DNA sequences to the human genome. *Genome Biol.* **10,** R25 (2009).
31. Anders, S. & Huber, W. Differential expression analysis for sequence count data. *Genome Biol.* **11,** R106 (2010).
32. Rouhana, L. *et al.* RNA interference by feeding *in vitro*-synthesized double-stranded RNA to planarians: methodology and dynamics. *Dev. Dyn.* **242,** 718–730 (2013).
33. Ross, K. G. *et al.* Novel monoclonal antibodies to study tissue regeneration in planarians. *BMC Dev. Biol.* **15,** 2 (2015).
34. Schierwater, B. *et al.* The early ANTP gene repertoire: insights from the placozoan genome. *PLoS One* **3,** e2457 (2008).
35. Fahey, B. & Degnan, B. M. Origin and evolution of laminin gene family diversity. *Mol. Biol. Evol.* **29,** 1823–1836 (2012).
36. Scimone, M. L., Kravarik, K. M., Lapan, S. W. & Reddien, P. W. Neoblast specialization in regeneration of the planarian *Schmidtea mediterranea*. *Stem Cell Reports* **3,** 339–352 (2014).

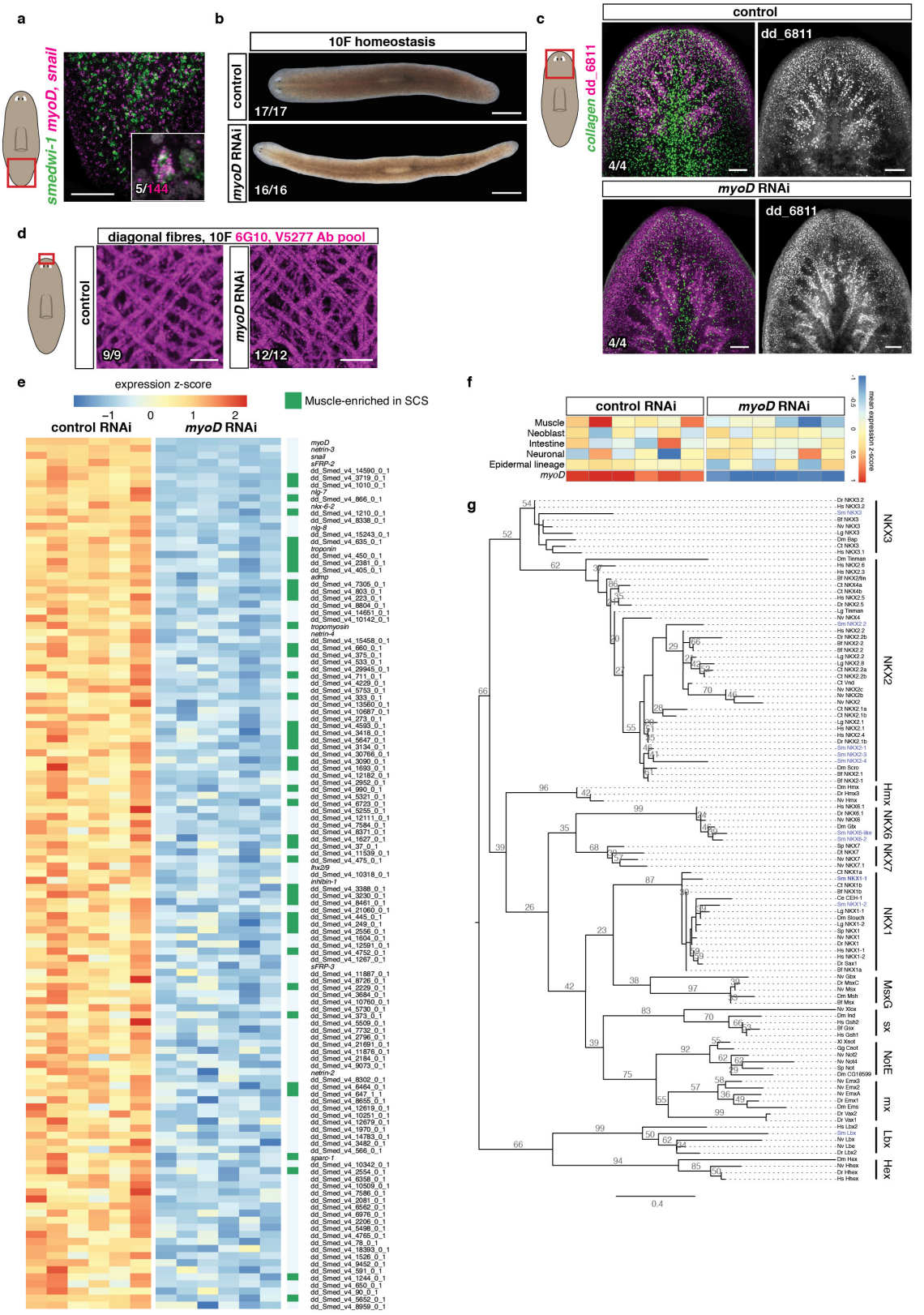

Extended Data Figure 1 | See next page for caption.

Extended Data Figure 1 | *myoD* is a myogenic gene in planarians that is specific for longitudinal muscle fibres. a, Co-expression of *myoD* (*myoD* and *snail* probes pooled) and the neoblast marker *smedwi-1* (five animals, two experiments; white, double-positive cells). **b**, Live image shows a longer and thinner *myoD*(*RNAi*) animal (quantification in Fig. 1c). **c**, Reduction in BWM (*collagen*$^{+}$) but not intestinal muscle (dd_6811^{+})[17] in an uninjured *myoD*(*RNAi*) animal after ten dsRNA feedings. **d**, *myoD* or control RNAi animals have comparable diagonal fibre numbers. Scale bars, 10 μm. **e**, Heat map shows genes downregulated ($\log_2$[fold change] < 0, adjusted P value < 0.001) in uninjured *myoD*(*RNAi*) animals. Green, muscle-enriched genes from single-cell RNA-seq data[17] (AUC > 0.8; 43 out of 123 genes). Each column is a replicate. **f**, Heat map showing that other tissue-enriched gene expression is not affected in *myoD*(*RNAi*) animals. Mean of tissue-enriched genes[17] (AUC > 0.8) is used. Each column is a replicate. **g**, Phylogenetic analysis of homeodomain transcription factors. Accession numbers are in Supplementary Table 2. Tree shows 105 proteins from diverse organisms. Maximum likelihood analyses were run using PhyML with 100 bootstrap replicates. All maximum likelihood bootstrap values >20 are shown. Bf: *Branchiostoma floridae*; Ce: *Caenorhabditis elegans*; Ct: *Capitella teleta*; Dm: *Drosophila melanogaster*; Dr: *Danio rerio*; Dt: *Discocelis tigrina*; Gg: *Gallus gallus*; Hs: *Homo sapiens*; Lg: *Lottia gigantea*; Nv: *Nematostella vectensis*; Od: *Oikopleura dioica*; Sm: *Schmidtea mediterranea*; Sp: *Strongylocentrotus purpuratus*; Xl: *Xenopus laevis*. The *lhx2/9* tree was previously reported[36]. All FISH panels are representative images of two independent experiments. Bottom left number: animals with phenotype out of total tested. Anterior, up. Scale bars, 100 μm unless indicated.

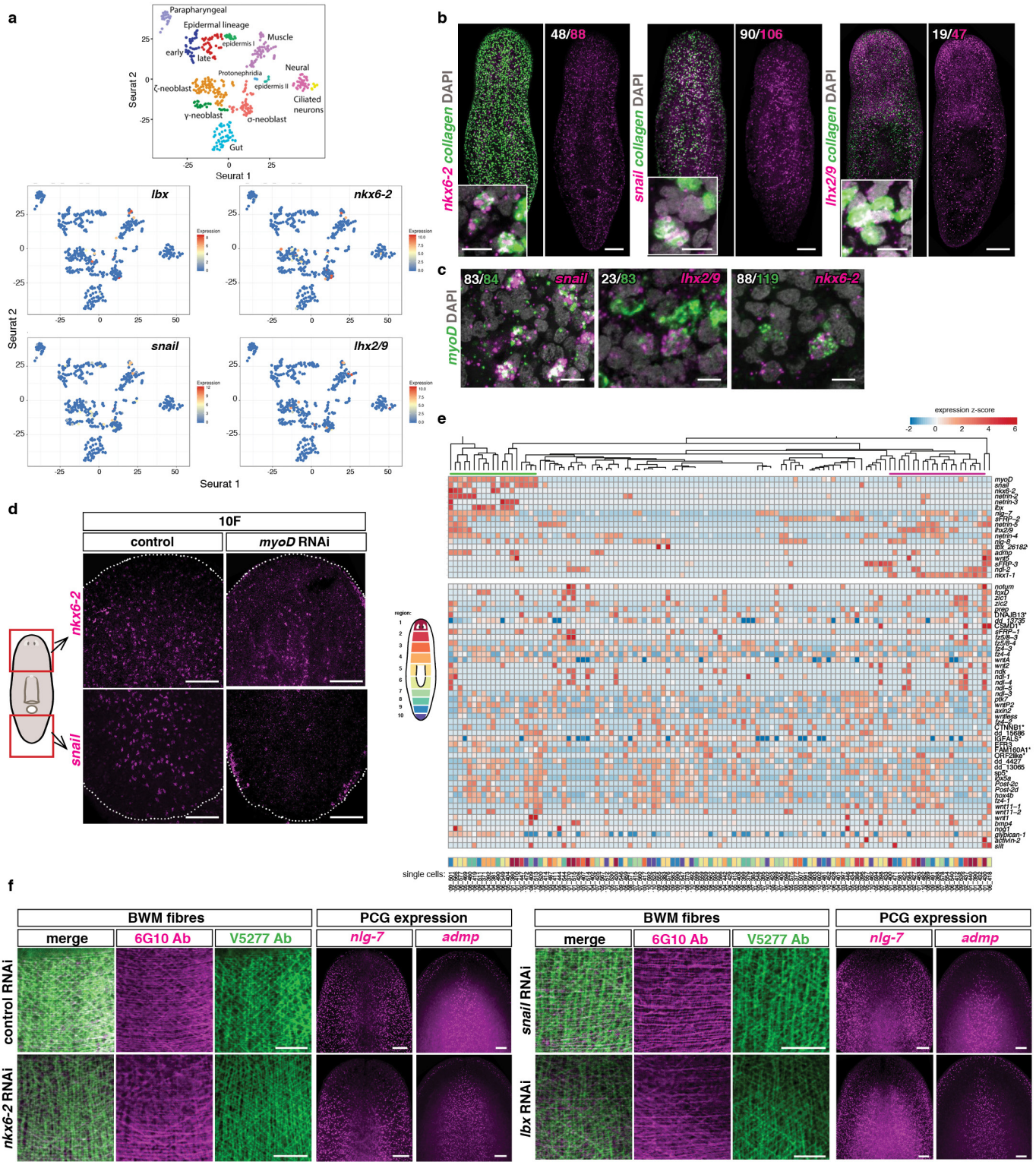

Extended Data Figure 2 | A subset of transcription factors is expressed in longitudinal muscle fibres. a, Seurat maps show expression of transcription factors downregulated in *myoD*(*RNAi*) animals within a reported[17] single-cell RNA-seq experiment. Each dot represents a cell. **b**, Co-expression of those transcription factors and the BWM marker *collagen* in uninjured animals. Scale bars, 100 μm; insets, 10 μm. Number of cells expressing both genes (white) within the total number of cells expressing the transcription factor (magenta) is shown (five animals, two experiments). **c**, Co-expression of *myoD* and transcription factors (white) within the total *myoD*$^+$ cells (green) in uninjured animals (five animals, two experiments). Scale bars, 10 μm. **d**, Reduced expression of transcription factors in uninjured *myoD*(*RNAi*) animals (five animals, two experiments). Scale bars, 100 μm. **e**, Heat map shows two clusters of muscle cells (*myoD*$^+$ and *nkx1-1*$^+$) and co-expression with other muscle transcription factors, PCGs and muscle regional expressed genes. Most PCG expression is widely distributed across all muscle cells. Each column is a single cell. Analyses using previously reported single-cell muscle data[27]. Asterisks denote best human BLAST hit. Cartoon shows in different colours the regions from which single muscle cell data were collected[27]. **f**, No major differences in BWM structure and expression of longitudinal fibre-enriched PCGs in the different RNAi conditions tested (10 dsRNA feedings, uninjured animals, five animals per group, two experiments). Scale bars, 50 μm. Anterior, up.

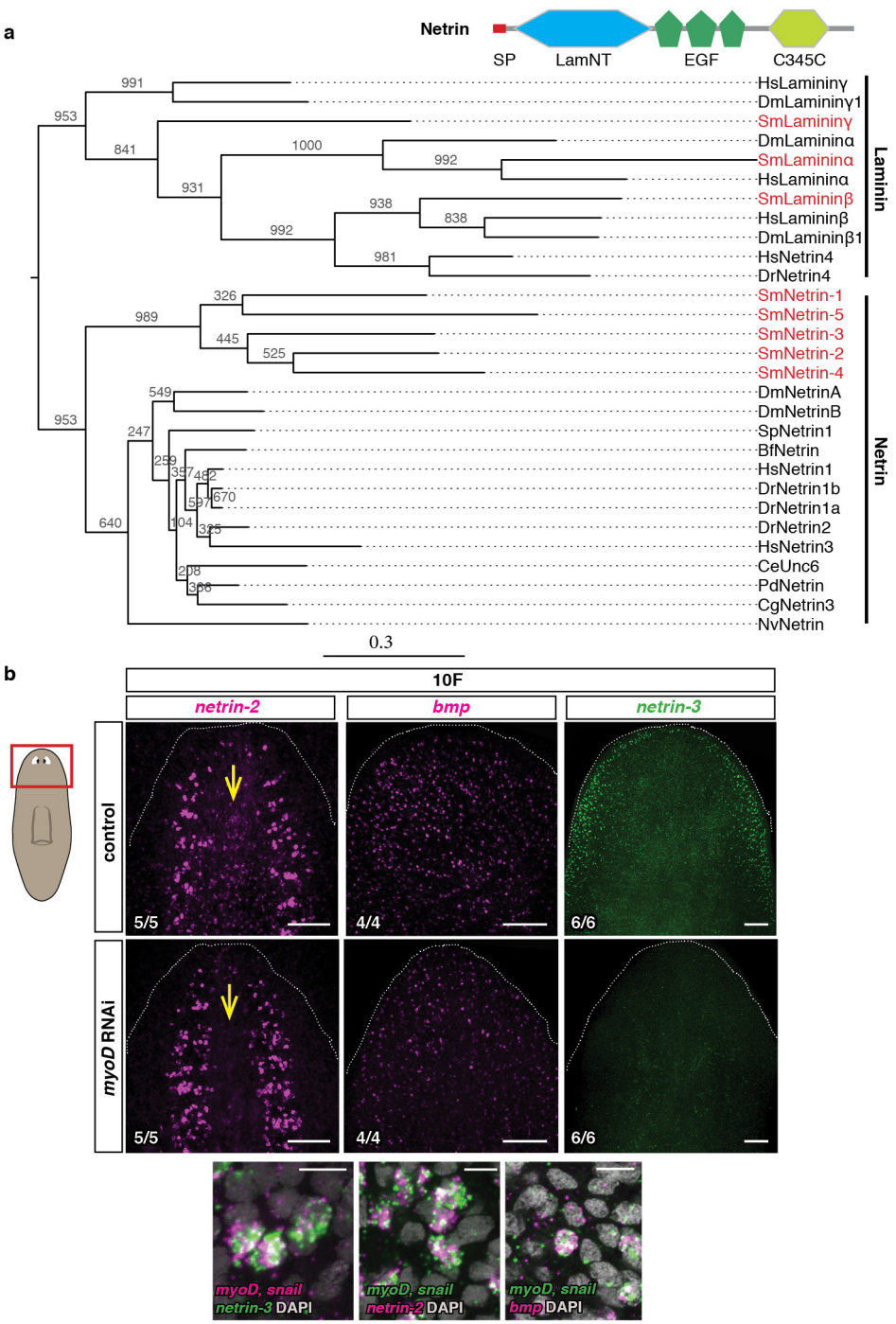

Extended Data Figure 3 | A subset of PCGs is enriched in longitudinal muscle fibres. a, Phylogenetic analysis of all planarian netrins. Accession numbers used for the tree are in Supplementary Table 2. Tree shows 20 Netrin proteins from diverse organisms, which were aligned using MUSCLE with default settings and trimmed with Gblocks. Maximum likelihood analyses were run using PhyML with 1,000 bootstrap replicates. All maximum likelihood bootstrap values are shown above or below the respective branch. Dm, *Drosophila melanogaster*; Sp, *Strongylocentrotus purpuratus*; Bf, *Branchiostoma floridae*; Hs, *Homo sapiens*; Dr, *Danio rerio*; Ce, *Caenorhabditis elegans*; Pd, *Platynereis dumerilii*; Cg, *Crassostrea gigas*; Sm, *Schmidtea mediterranea*; Nv, *Nematostella vectensis*. Cartoon shows protein domain structure. **b**, Reduced expression of PCGs following *myoD* RNAi and co-expression of pooled *myoD* and *snail* with those PCGs in uninjured animals. Scale bars, 100 μm (top panels), 10 μm (bottom panels). Red box in left cartoon depicts location of image shown. FISH images are representative of two independent experiments. Bottom left number: animals with phenotype out of total tested. Anterior, up.

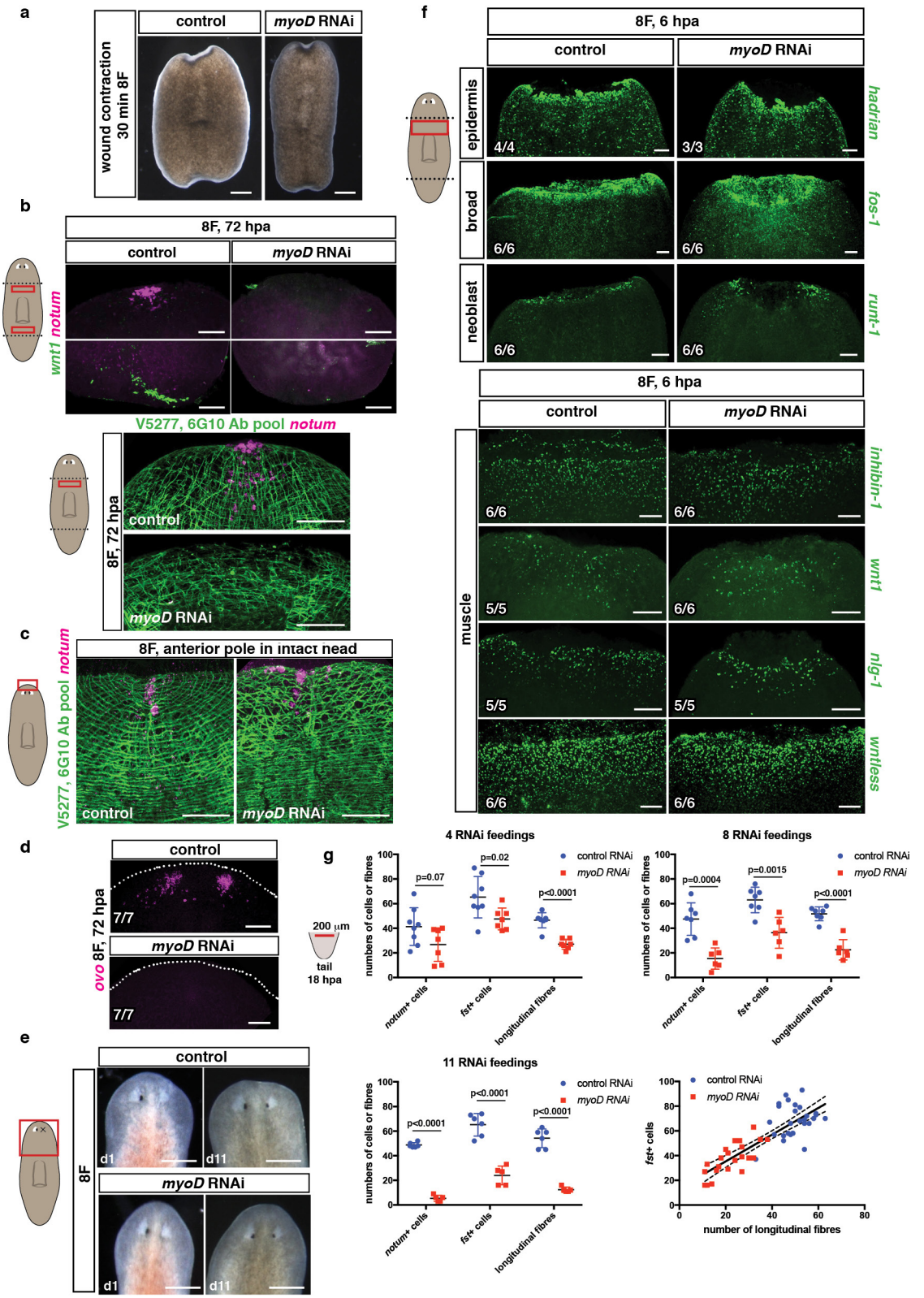

Extended Data Figure 4 | *myoD* is required for regeneration. **a**, Normal wound contraction in *myoD*(*RNAi*) animals. Trunk fragments are shown 30 min after amputation (15 animals, 3 experiments). **b**, Lack of anterior (*notum*$^+$) and posterior (*wnt1*$^+$) pole cells (top) and BWM structure (bottom) at 72 hpa during regeneration in *myoD*(*RNAi*) animals. **c**, Anterior pole (*notum*$^+$) and BWM structure in uninjured animals (**b**, **c**; ten animals per group, three experiments). Scale bars, 50 µm. **d**, Neoblasts did not specify into eye progenitors (*ovo*$^+$) in *myoD*(*RNAi*) animals at 72 hpa (one experiment). **e**, Homeostatic eye replacement 11 days after eye resection in *myoD*(*RNAi*) animals (ten animals per group, one experiment). Scale bars, 500 µm. **f**, Normal epidermis, neoblast and muscle expression of wound-induced genes in *myoD*(*RNAi*) animals 6 hpa. **g**, Graphs show reduced numbers of *notum*$^+$ and *fst*$^+$ cells and longitudinal fibres in *myoD*(*RNAi*) animals at 18 hpa after different numbers of dsRNA feedings. Cartoon shows the region counted. Linear correlation between *fst*$^+$ cells and longitudinal fibres. Regression coefficient, $R^2 = 0.6928$. Two-tailed Student's *t*-test was performed. *P* values are shown in graphs. Mean ± s.d. shown in all graphs. Bottom left number: animals with phenotype out of total tested. Anterior, up. Scale bars, 100 µm unless indicated.

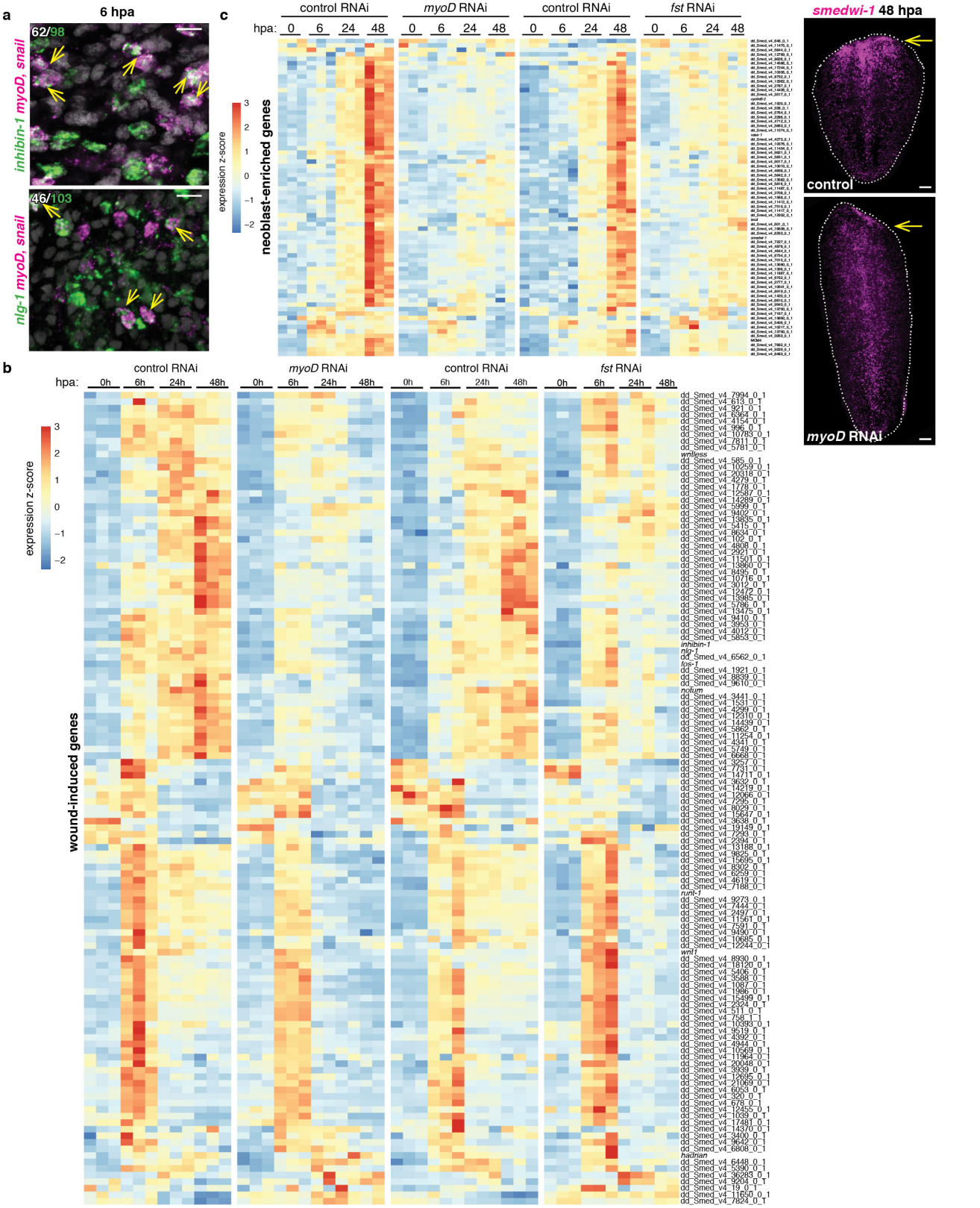

Extended Data Figure 5 | *myoD* is required for the regenerative response. a, Partial co-expression of *myoD* (*myoD* and *snail* probes pooled) and muscle-wound induced genes *inhibin-1* and *nlg-1* at 6 hpa (four animals, one experiment). Number in white indicates co-expression within total number of counted cells expressing the wound-induced gene (green). Scale bars, 10 μm. **b**, Heat map shows expression of all 128 wound-induced genes[17] from anterior-facing wounds of regenerating tail fragments of control, *myoD* and *fst* RNAi animals at different time points after amputation. Each column is a replicate. **c**, Heat map shows expression of neoblast genes[17] (AUC > 0.8) in anterior-facing wounds of regenerating tail fragments of control, *myoD* and *fst* RNAi animals at different time points after amputation. Each column is a replicate. Right, no neoblast (*smedwi-1*$^{+}$) accumulation at wounds (yellow arrow) 48 hpa in *myoD*(*RNAi*) tail fragments after eight dsRNA feedings (six animals, one experiment).

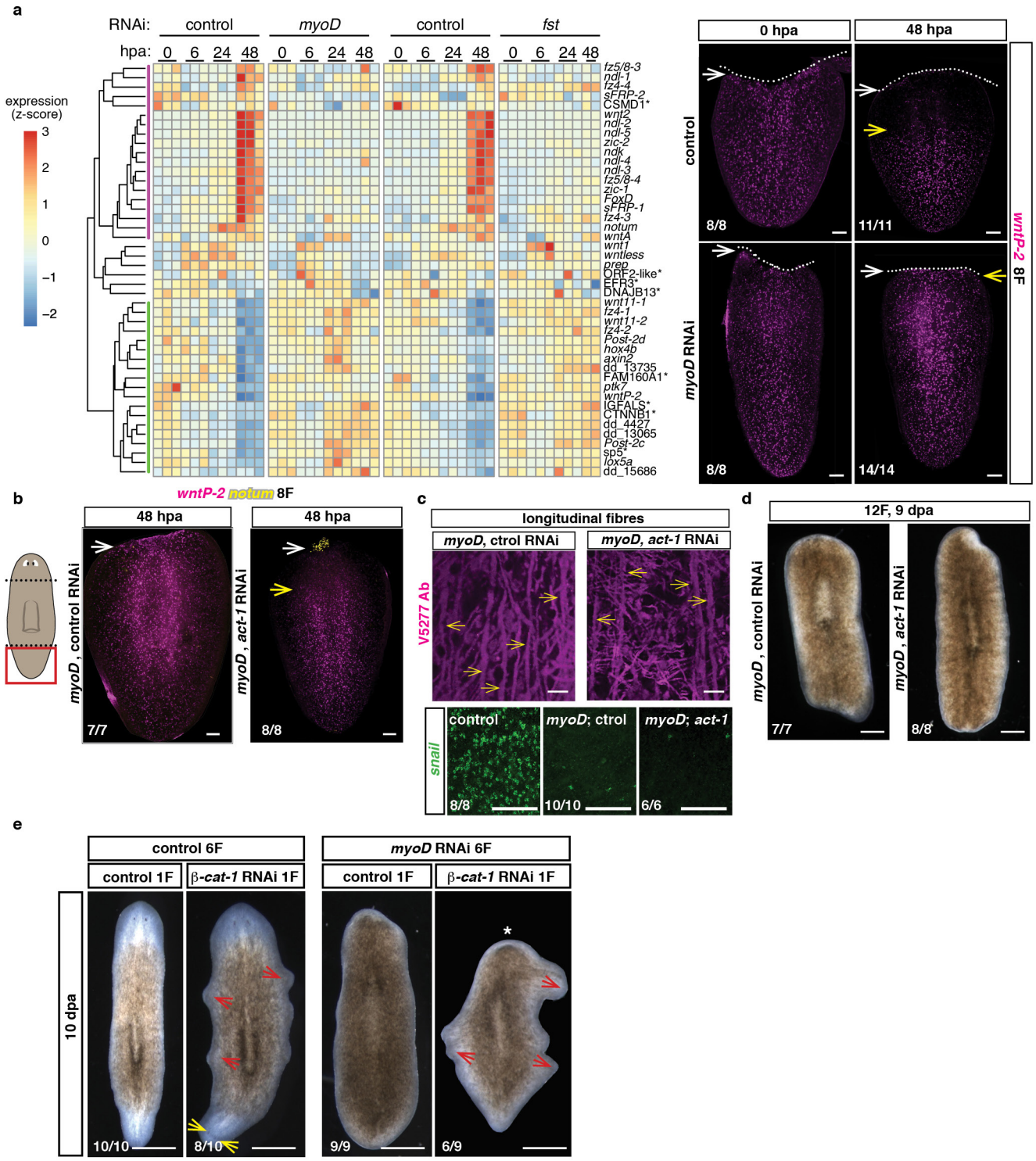

Extended Data Figure 6 | The lack of a regenerative response in *myoD(RNAi)* animals is suppressed by *act-1* inhibition. a, Heat map shows failure to re-scale posterior or initiate expression of anterior regionally expressed muscle genes defined in a previous study[27] in tail fragments of *myoD* and *fst* RNAi animals. Each column represents a replicate. Asterisks denote best human BLAST hit. Right, failure to re-scale *wntP-2* in tail fragments of *myoD(RNAi)* animals at 48 hpa (eight animals for control, ten animals for *myoD* RNAi, three experiments). White arrows point to wound site, yellow arrows point to *wntP-2* expression. Dotted line indicates wound site. **b**, Re-scaling of *wntP-2* and expression of anterior pole cells (*notum*$^{+}$) in tail fragments of double *myoD* and *act-1* RNAi animals at 48 hpa (two experiments). White arrows point to wound site, yellow arrows point to *wntP-2* expression. **c**, Comparable loss of longitudinal fibres (yellow arrows) in both groups (*myoD* and control RNAi animals, and *myoD* and *act-1* RNAi animals; quantification in Fig. 2i). Scale bars, 10 μm. Loss of *snail* expression in both groups (two experiments). **d**, Long-term double *myoD;* control and *myoD; act-1* RNAi animals failed to regenerate (two experiments). **e**, *β-catenin-1* inhibition did not suppress the regeneration defect of *myoD(RNAi)* animals (one experiment). However, homeostatic ectopic stretching head-like outgrowths (red arrows) formed around the periphery of *β-catenin-1(RNAi)* animals. Asterisk denotes absence of anterior blastema, yellow arrows point to ectopic eyes. Bottom left number, animals with phenotype out of total tested. Anterior, up. Scale bars, 100 μm unless indicated.

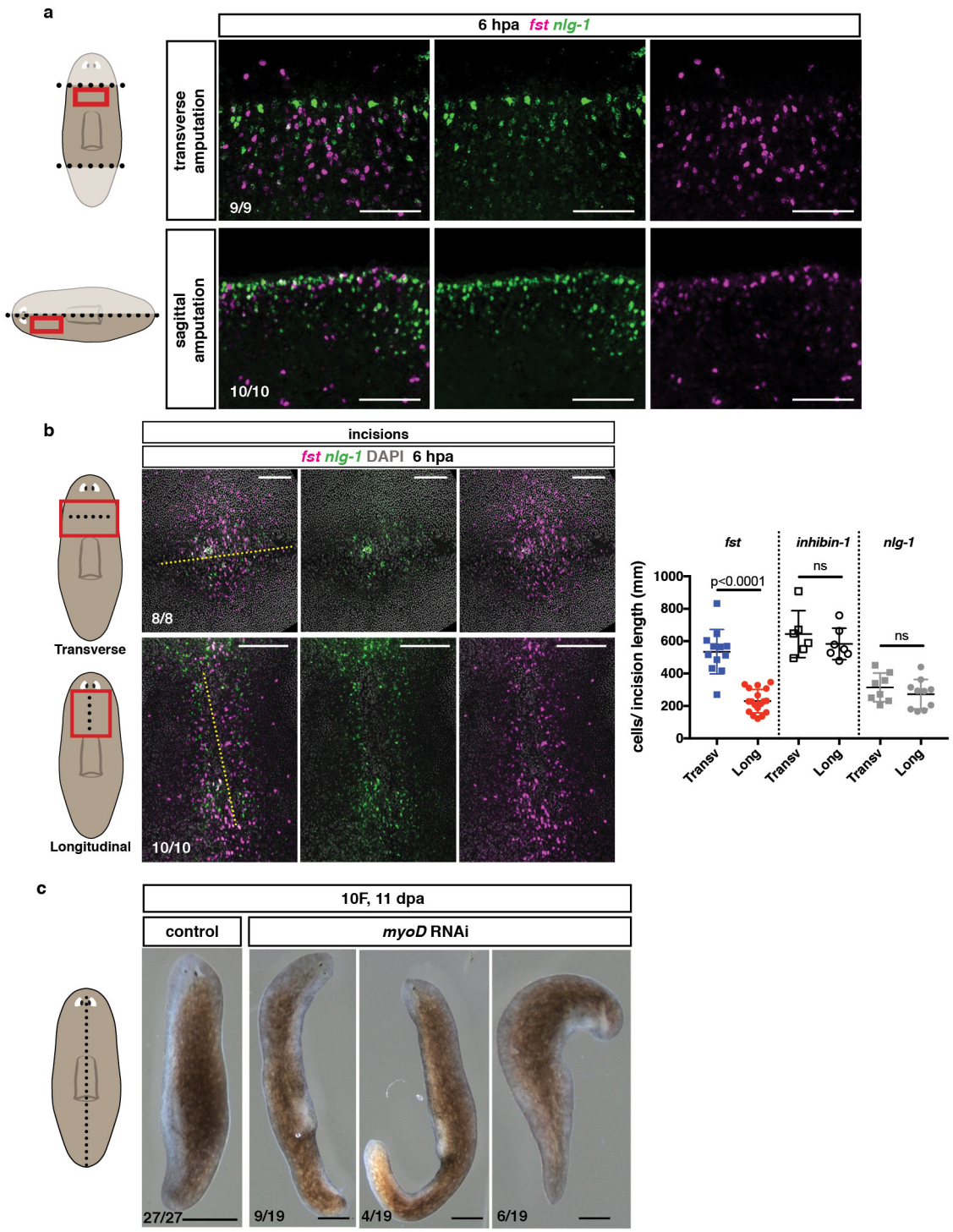

Extended Data Figure 7 | Transverse injuries trigger more *fst* expression than longitudinal injuries. a, Higher numbers of *fst*$^{+}$ cells relative to *nlg-1*$^{+}$ cells in transverse versus sagittal amputations at 6 hpa. **b**, Higher numbers of wound-induced *fst*$^{+}$ cells relative to *nlg-1*$^{+}$ cells in transverse versus longitudinal incisions at 6 hpa. Yellow dotted lines show site of incision. Right graph shows total numbers of *fst*$^{+}$, *inhibin-1*$^{+}$ and *nlg-1*$^{+}$ cells per length of wound at 6 hpa. Two-tailed Student's *t*-test was performed. Mean ± s.d. are shown. ns, not significant. *P* values are shown. Red box in cartoon depicts location of image shown; dotted line, plane of injury performed. **c**, Live images show that *myoD*(*RNAi*) animals regenerated small blastemas following sagittal amputations (three experiments). Scale bars, 500 μm. All FISH and live images shown are anterior, up. Bottom left number, animals with phenotype out of total tested. Scale bars, 100 μm unless indicated.

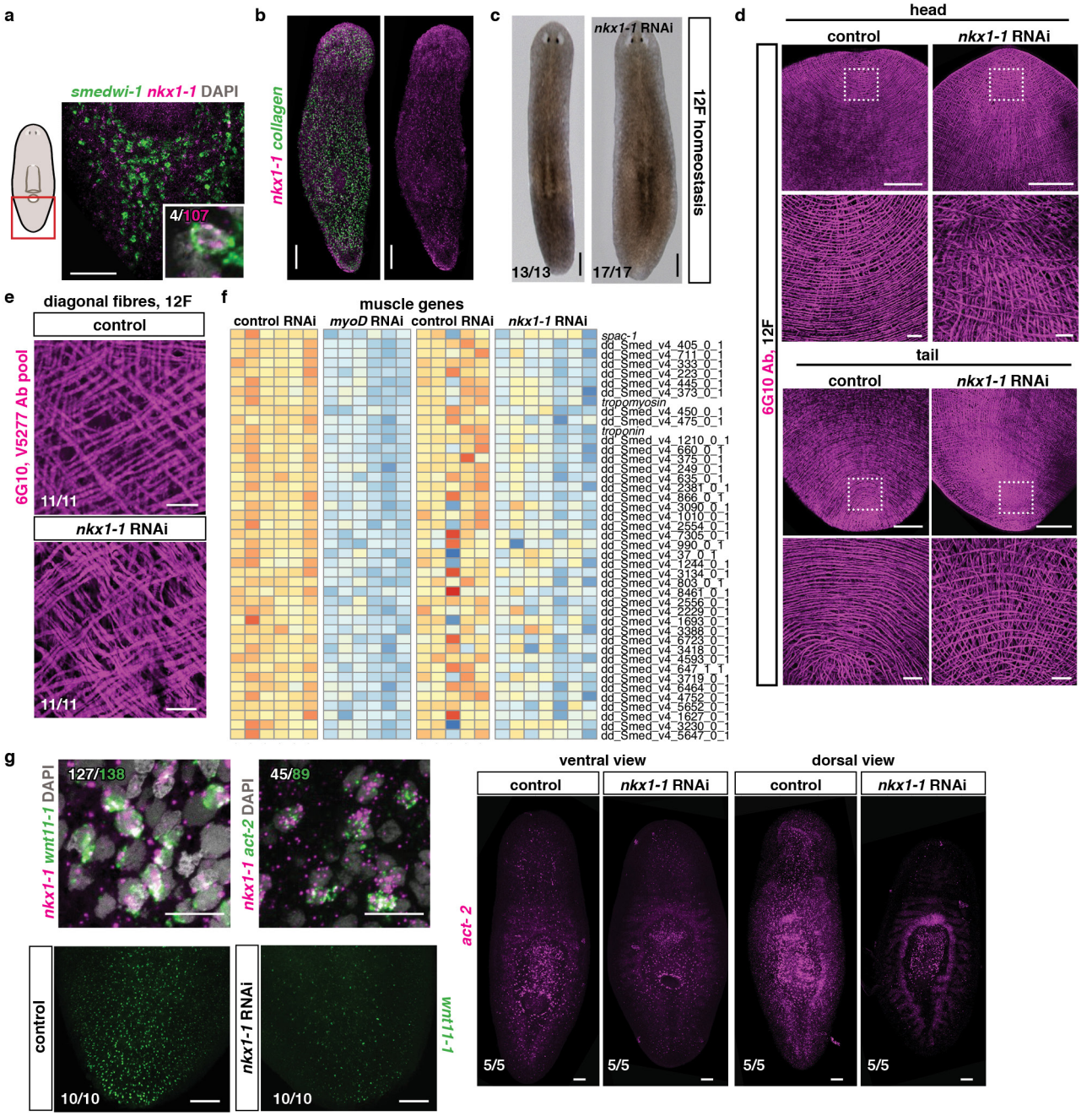

Extended Data Figure 8 | *nkx1-1* specifies circular muscle fibres. **a**, A minor fraction of *nkx1-1*$^{+}$ cells co-expresses the neoblast marker *smedwi-1*. **b**, Expression of *nkx1-1* within the *collagen*$^{+}$ BWM in an uninjured animal (five animals, two experiments (**a**, **b**)). **c**, Animals become wider after *nkx1-1* RNAi (quantification in Fig. 3b, 13 control and 17 *nkx1-1* RNAi animals, three experiments). **d**, Loss of circular fibres in *nkx1-1*(*RNAi*) animals (quantification in Fig. 3c). Scale bars in expanded views, 10 μm. **e**, Comparable numbers of diagonal fibres in *nkx1-1* and control RNAi animals (three experiments). Scale bars, 10 μm. **f**, Heat map shows 43 muscle-enriched genes downregulated ($\log_2$[fold change] < 0, adjusted *P* value < 0.001) in both uninjured *myoD* and *nkx1-1* RNAi animals. Each column represents a replicate. **g**, Co-expression of *nkx1-1* and PCGs (top) and reduced PCG expression in uninjured *nkx1-1*(*RNAi*) animals after 12 dsRNA feedings. Numbers in white indicate double-positive cells within the total number of counted cells expressing the PCG (green) (three experiments). Red box on cartoons depicts location of image shown. Bottom left number, animals with phenotype out of total tested. Anterior, up. Scale bars, 100 μm unless indicated.

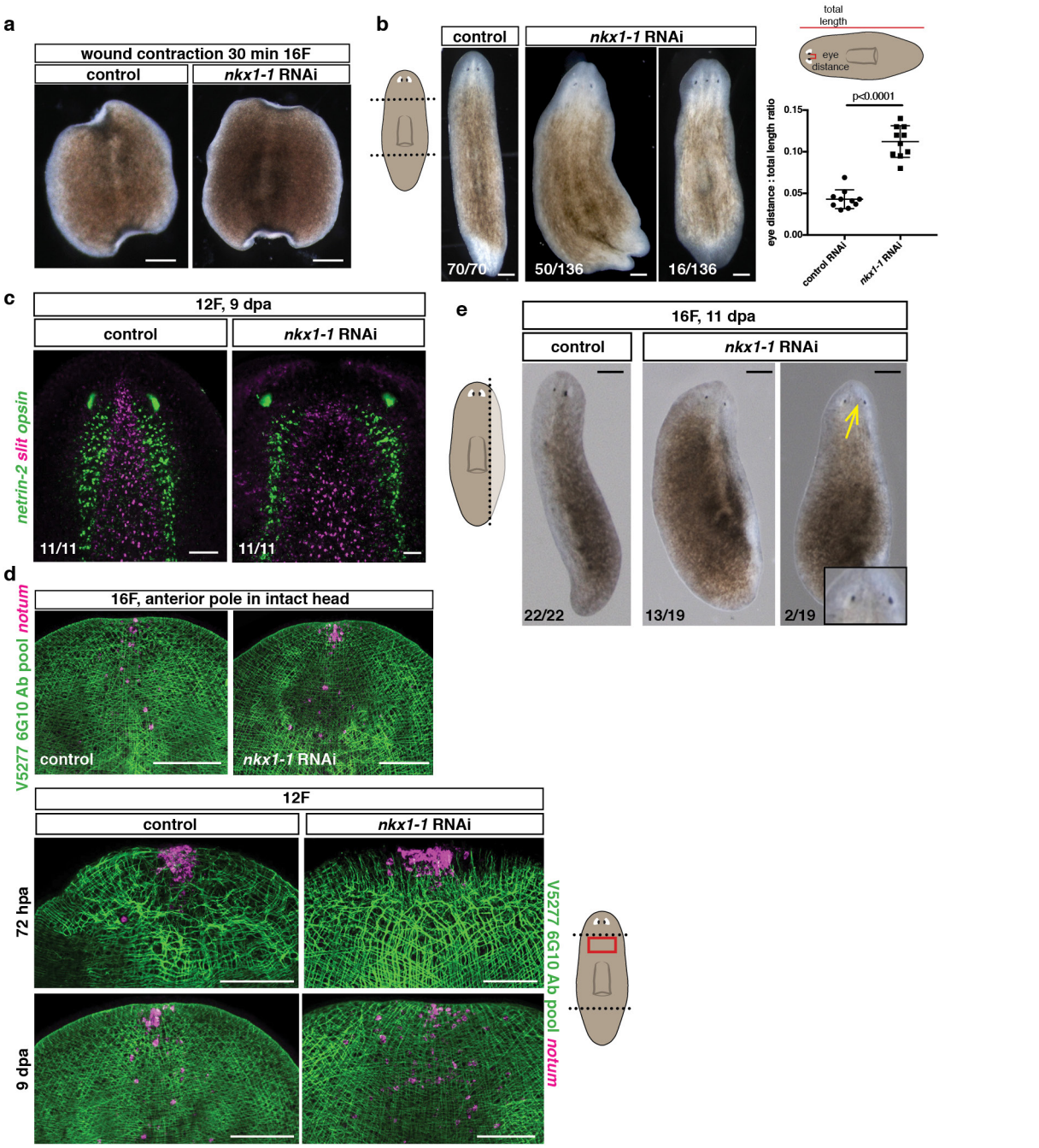

Extended Data Figure 9 | *nkx1-1* is required for normal medial–lateral patterning during regeneration. a, Normal wound contraction in *nkx1-1*(*RNAi*) animals. Trunk fragments are shown 30 min after amputation (15 animals, three experiments). **b**, Live images of regenerating (9–14 dpa) *nkx1-1*(*RNAi*) animals after 12 dsRNA feedings following a transverse amputation (five experiments). Scale bars, 500 μm. Graph shows quantification of eye distance relative to total animal length (ten animals per group, two experiments). Two-tailed Student's *t*-test was performed. Mean ± s.d. are shown. Lines in cartoon on top show where the measurements were taken. **c**, Increased width of midline (*slit*) and brain lobes (*netrin-2*) in *nkx1-1*(*RNAi*) animals (three experiments). **d**, Anterior pole (*notum*$^{+}$) and BWM fibres in intact (top) and regenerating (bottom, 72 hpa and 9 dpa) *nkx1-1*(*RNAi*) animals (12 animals per group, two experiments). **e**, Live images of regenerating *nkx1-1*(*RNAi*) animals following a sagittal amputation (three experiments). Yellow arrow points to ectopic eye. Scale bars, 200 μm. Dotted lines in cartoons show amputation sites. Red box in cartoons depicts location of image shown. All FISH and live images shown are anterior, up. Bottom left number, animals with phenotype out of total tested. Scale bars, 100 μm, unless indicated.

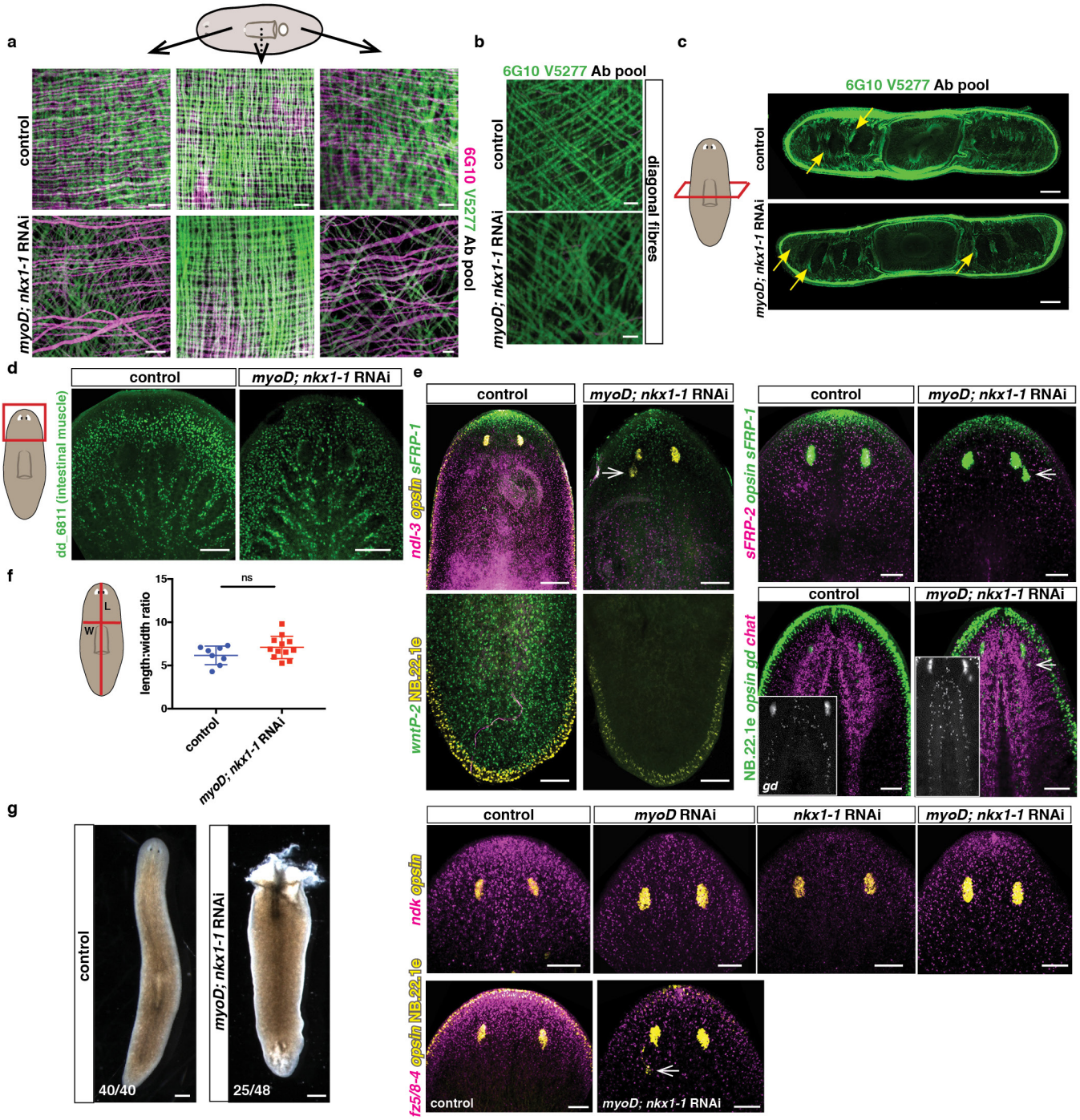

Extended Data Figure 10 | Longitudinal and circular muscle fibres are required for normal patterning during homeostatic tissue turnover. **a**, Reduced numbers of longitudinal and circular muscle fibres but comparable numbers of pharynx muscle fibres in control and double *myoD* and *nkx1-1* RNAi animals. Dotted line in cartoon indicates that pharynx muscle is more internal than the BWM fibres (ten animals per group, three experiments). Scale bars, 10 μm. **b**, Comparable numbers of diagonal fibres in control and double *myoD* and *nkx1-1* RNAi animals (ten animals per group, three experiments). Scale bars, 10 μm. **c**, Cross sections showing comparable dorsal–ventral fibres (yellow arrows) in control and double *myoD* and *nkx1-1* RNAi animals (eight animals per group, two experiments). **d**, Intestinal muscle (dd_6811) is not affected in double *myoD* and *nkx1-1* RNAi animals (six animals per group, two experiments). **e**, Ectopic posterior eyes (*opsin*$^{+}$, white arrows) and reduced expression of PCGs (anterior: *sFRP-1*, *ndk*, *fz5/8-4*; midbody: *ndl-3* and *sFRP-2*; posterior: *wntP-2*) in double *myoD* and *nkx1-1* RNAi animals compared to controls (four animals per FISH, two experiments). Elongated brain lobes were also observed in double *myoD* and *nkx1-1* RNAi animals compared to controls (*chat*$^{+}$ and *gd*$^{+}$ cells). NB.22.1e marks epidermal cells at the boundary of the animals (five animals per group, two experiments). **f**, Graph shows similar length-to-width ratios in double *myoD* and *nkx1-1* RNAi animals and control RNAi animals (eight for control, twelve for double RNAi, two experiments). Two-tailed Student's *t*-test was performed. Mean ± s.d. are shown. Red lines in cartoon indicate where measurements were taken. **g**, Live image of a dying double *myoD* and *nkx1-1* RNAi animal. Lysis occurs 12–20 weeks after first dsRNA feeding. Scale bars, 500 μm. Red box in cartoons depicts location of image shown. All FISH and live images shown are anterior, up. Bottom left number, animals with phenotype out of total tested. Scale bars, 100 μm unless indicated.

Extended Data Table 1 | Summary of patterning gene expression in different muscle fibre types by *in situ* hybridization

Name	Contig	Co-expression in *myoD+* fibres	Co-expression in *nkx1-1+* fibres	Markedly reduced in *myoD(RNAi)* animals	Markedly reduced in *nkx1-1(RNAi)* animals	Markedly reduced in double *myoD, nkx1-1(RNAi)* animals
Smed-ndl-2	dd_Smed_v4_8340_0_1	Some	Some	no	no	yes
Smed-ndl-3	dd_Smed_v4_6604_0_1	na	na	no	na	yes
Smed-sFRP-1	dd_Smed_v4_13985_0_1	na	na	no	no	no
Smed_wnt11-2	dd_Smed_v4_16209_0_1	na	na	na	na	yes
Smed-wnt11-1	dd_Smed_v4_14391_0_1	None	High	no	yes	yes
Smed-wntP-2	dd_Smed_v4_7326_0_1	Some	Some	no	na	yes
Smed-netrin-2	dd_Smed_v4_14852_0_1	High	nd	yes	no	na
Smed-nlg-7	dd_Smed_v4_10469_0_1	High	Low	yes	no	na
Smed-bmp	dd_Smed_v4_17402_0_1	Some	Some	some reduction	no	yes
Smed-netrin-1	dd_Smed_v4_9795_0_1	Low	Some	no	no	na
Smed-wnt2	dd_Smed_v4_13487_0_1	na	na	na	no	na
Smed-act-2	dd_Smed_v4_3324_0_1	na	High	na	yes	na
Smed-nlg-8	dd_Smed_v4_8738_0_1	Some	Some	na	no	na
Smed-SFRP-2	dd_Smed_v4_8832_0_1	na	na	na	no	yes
Smed-netrin-3	dd_Smed_v4_18181_0_1	High	nd	yes	no	na
Smed-slit	dd_Smed_v4_12111_0_1	Some	nd	yes	no	na
Smed-admp	dd_Smed_v4_12939_2_1	High	Low	yes	no	na
Smed-netrin-5	dd_Smed_v4_9737_0_1	Low	Some	no	no	na
Smed-inhibin-1	dd_Smed_v4_7607_0_1	Some (wi)	Some (wi)	no	no	na
Smed-nlg-1	dd_Smed_v4_14068_0_1	Some (wi)	Some (wi)	no	no	na
Smed-notum	dd_Smed_v4_24180_0_1	High (wi)	nd	yes	na	na
Smed-fst	dd_Smed_v4_9584_0_1	High (wi)	nd	yes	na	na
Smed-wntless	dd_Smed_v4_11629_0_1	Some (wi)	Some (wi)	no	na	na

nd: not determined

na: not assayed

wi: wound-induced

nature research

Corresponding author(s): Peter W. Reddien

☐ Initial submission ☐ Revised version ☒ Final submission

Life Sciences Reporting Summary

Nature Research wishes to improve the reproducibility of the work that we publish. This form is intended for publication with all accepted life science papers and provides structure for consistency and transparency in reporting. Every life science submission will use this form; some list items might not apply to an individual manuscript, but all fields must be completed for clarity.

For further information on the points included in this form, see Reporting Life Sciences Research. For further information on Nature Research policies, including our data availability policy, see Authors & Referees and the Editorial Policy Checklist.

Experimental design

1. Sample size

Describe how sample size was determined.

Visual estimation of preliminary experiments indicated large effect sizes with greater than 2-fold differences on number of fibers and length-to-width ratios, therefore a minimum sample size of 6 was chosen to give a 99% power with a 1% false positive error rate. This size estimation applies for measurements taken in Figure 1c,d, Figure 2i, Figure 3b,c and Extended Data Figure 4g, Extended Data Figure 9b, and Extended Data Figure 10f. For RNA-sequencing of pooled wound sites, biological triplicates were used as in Wurtzel et al, 2015 and for whole animal RNA-seq, six animals were used instead to increase statistical power.

2. Data exclusions

Describe any data exclusions.

All animals were included in the analysis. For the sequencing data, one biological replicate was excluded from analysis and the explanation is in Methods.

3. Replication

Describe whether the experimental findings were reliably reproduced.

All experimental findings were reproduced at least in two independent experiments.

4. Randomization

Describe how samples/organisms/participants were allocated into experimental groups.

Animals for all experiments were randomly selected from a large collection of clonal animals for all experiments.

5. Blinding

Describe whether the investigators were blinded to group allocation during data collection and/or analysis.

Investigators were not blinded during data collection and analysis.

Note: all studies involving animals and/or human research participants must disclose whether blinding and randomization were used.

6. Statistical parameters

For all figures and tables that use statistical methods, confirm that the following items are present in relevant figure legends (or in the Methods section if additional space is needed).

n/a	Confirmed
☐	☒ The exact sample size (*n*) for each experimental group/condition, given as a discrete number and unit of measurement (animals, litters, cultures, etc.)
☐	☒ A description of how samples were collected, noting whether measurements were taken from distinct samples or whether the same sample was measured repeatedly
☐	☒ A statement indicating how many times each experiment was replicated
☐	☒ The statistical test(s) used and whether they are one- or two-sided (note: only common tests should be described solely by name; more complex techniques should be described in the Methods section)
☐	☒ A description of any assumptions or corrections, such as an adjustment for multiple comparisons
☐	☒ The test results (e.g. *P* values) given as exact values whenever possible and with confidence intervals noted
☐	☒ A clear description of statistics including central tendency (e.g. median, mean) and variation (e.g. standard deviation, interquartile range)
☐	☒ Clearly defined error bars

See the web collection on statistics for biologists for further resources and guidance.

Software

Policy information about availability of computer code

7. Software

Describe the software used to analyze the data in this study.	Prism 7 was used for all statistical analysis. Zeiss ZEN was used for image acquisition and ImageJ was used for contrast adjustment and cell counting. bowtie 1 was used for mapping reads. R packages DESeq and pheatmap were used to analyze differential expression between conditions and to generate scaled heatmaps. MUSCLE was used to align protein sequences. PhyML was used to calculate phylogenetic trees which were then visualized in FigTree. Further details and citations are in Methods.

For manuscripts utilizing custom algorithms or software that are central to the paper but not yet described in the published literature, software must be made available to editors and reviewers upon request. We strongly encourage code deposition in a community repository (e.g. GitHub). *Nature Methods* guidance for providing algorithms and software for publication provides further information on this topic.

Materials and reagents

Policy information about availability of materials

8. Materials availability

Indicate whether there are restrictions on availability of unique materials or if these materials are only available for distribution by a for-profit company.	No restrictions

9. Antibodies

Describe the antibodies used and how they were validated for use in the system under study (i.e. assay and species).	The antibodies used were monoclonal (mouse 6G10 (DSHB; Ross et al, 2014)) and polyclonal rabbit V5277; these recognized unknown epitopes in planarian muscle. The stained structures in S. mediterranea were identified as planarian muscle by the very distinct, well-established appearance of muscle, similarity of the staining to f-actin (phalloidin) staining, and similarity to anti-planarian MHC (TMUS13) staining.

10. Eukaryotic cell lines

a. State the source of each eukaryotic cell line used.	n/a
b. Describe the method of cell line authentication used.	n/a
c. Report whether the cell lines were tested for mycoplasma contamination.	n/a
d. If any of the cell lines used are listed in the database of commonly misidentified cell lines maintained by ICLAC, provide a scientific rationale for their use.	n/a

Animals and human research participants

Policy information about studies involving animals; when reporting animal research, follow the ARRIVE guidelines

11. Description of research animals

Provide details on animals and/or animal-derived materials used in the study.	A clonal asexual line (CIW4) of planarians was used.

Policy information about studies involving human research participants

12. Description of human research participants

Describe the covariate-relevant population characteristics of the human research participants.	n/a